U.S. Department of
Transportation
**Federal Railroad
Administration**

Retrofit and Full-Scale Testing of a State-of-the-Art End Structure on a Budd M1 Cab Car

Office of Research.
Development,
and Technology
Washington, DC 20590

REPORT DOCUMENTATION PAGE

Form Approved
OMB No. 0704-0188

Public reporting burden for this collection of information is estimated to average 1 hour per response, including the time for reviewing instructions, searching existing data sources, gathering and maintaining the data needed, and completing and reviewing the collection of information. Send comments regarding this burden estimate or any other aspect of this collection of information, including suggestions for reducing this burden, to Washington Headquarters Services, Directorate for Information Operations and Reports, 1215 Jefferson Davis Highway, Suite 1204, Arlington, VA 22202-4302, and to the Office of Management and Budget, Paperwork Reduction Project (0704-0188), Washington, DC 20503.

1. AGENCY USE ONLY (Leave blank)	2. REPORT DATE August 2021	3. REPORT TYPE AND DATES COVERED Final Report July 2007 – July 2009

4. TITLE AND SUBTITLE Retrofit and Full-Scale Testing of a State-of-the-Art End Structure on a Budd M1 Cab Car	5. FUNDING NUMBERS DTRS57-04-D-30008
6. AUTHOR(S) Dr. Richard Stringfellow	

7. PERFORMING ORGANIZATION NAME(S) AND ADDRESS(ES) TIAX LLC 35 Hartwell Avenue Lexington, MA 02421-3102	8. PERFORMING ORGANIZATION REPORT NUMBER DOT-VNTSC-FRA-XX-XX

9. SPONSORING/MONITORING AGENCY NAME(S) AND ADDRESS(ES) U.S. Department of Transportation Federal Railroad Administration Office of Railroad Policy and Development Office of Research, Development and Technology Washington, DC 20590 — U.S. Department of Transportation Volpe National Transportation Systems Center 55 Broadway, Cambridge, MA 02142	10. SPONSORING/MONITORING AGENCY REPORT NUMBER DOT/FRA/ORD-21/23

11. SUPPLEMENTARY NOTES
COR: Michelle Muhlanger (Volpe)

12a. DISTRIBUTION/AVAILABILITY STATEMENT This document is available to the public through the FRA website.	12b. DISTRIBUTION CODE

13. ABSTRACT

This report describes the results of a program to modify the existing state-of-the-art end structure design for a Budd Pioneer cab car so it can be installed on a Budd M1 car and used to test the performance of end frames built to meet current APTA and proposed Federal Railroad Administration (FRA) structural requirements. The research was performed as part of the Equipment Safety Research Program sponsored by the FRA Office of Research, Development, and Technology.

14. SUBJECT TERMS End structure, crashworthiness, retrofit, dynamic testing, quasi-static testing, finite element analysis, cab car, impacts, rail cars, collision.	15. NUMBER OF PAGES 87
	16. PRICE CODE

17. SECURITY CLASSIFICATION OF REPORT Unclassified	18. SECURITY CLASSIFICATION OF THIS PAGE Unclassified	19. SECURITY CLASSIFICATION OF ABSTRACT Unclassified	20. LIMITATION OF ABSTRACT Unlimited

i

METRIC/ENGLISH CONVERSION FACTORS

ENGLISH TO METRIC

LENGTH (APPROXIMATE)

1 inch (in)	=	2.5 centimeters (cm)
1 foot (ft)	=	30 centimeters (cm)
1 yard (yd)	=	0.9 meter (m)
1 mile (mi)	=	1.6 kilometers (km)

AREA (APPROXIMATE)

1 square inch (sq in, in²)	=	6.5 square centimeters (cm²)
1 square foot (sq ft, ft²)	=	0.09 square meter (m²)
1 square yard (sq yd, yd²)	=	0.8 square meter (m²)
1 square mile (sq mi, mi²)	=	2.6 square kilometers (km²)
1 acre = 0.4 hectare (he)	=	4,000 square meters (m²)

MASS - WEIGHT (APPROXIMATE)

1 ounce (oz)	=	28 grams (gm)
1 pound (lb)	=	0.45 kilogram (kg)
1 short ton = 2,000 pounds (lb)	=	0.9 tonne (t)

VOLUME (APPROXIMATE)

1 teaspoon (tsp)	=	5 milliliters (ml)
1 tablespoon (tbsp)	=	15 milliliters (ml)
1 fluid ounce (fl oz)	=	30 milliliters (ml)
1 cup (c)	=	0.24 liter (l)
1 pint (pt)	=	0.47 liter (l)
1 quart (qt)	=	0.96 liter (l)
1 gallon (gal)	=	3.8 liters (l)
1 cubic foot (cu ft, ft³)	=	0.03 cubic meter (m³)
1 cubic yard (cu yd, yd³)	=	0.76 cubic meter (m³)

TEMPERATURE (EXACT)

$[(x-32)(5/9)]\ °F = y\ °C$

METRIC TO ENGLISH

LENGTH (APPROXIMATE)

1 millimeter (mm)	=	0.04 inch (in)
1 centimeter (cm)	=	0.4 inch (in)
1 meter (m)	=	3.3 feet (ft)
1 meter (m)	=	1.1 yards (yd)
1 kilometer (km)	=	0.6 mile (mi)

AREA (APPROXIMATE)

1 square centimeter (cm²)	=	0.16 square inch (sq in, in²)
1 square meter (m²)	=	1.2 square yards (sq yd, yd²)
1 square kilometer (km²)	=	0.4 square mile (sq mi, mi²)
10,000 square meters (m²)	=	1 hectare (ha) = 2.5 acres

MASS - WEIGHT (APPROXIMATE)

1 gram (gm)	=	0.036 ounce (oz)
1 kilogram (kg)	=	2.2 pounds (lb)
1 tonne (t)	=	1,000 kilograms (kg)
	=	1.1 short tons

VOLUME (APPROXIMATE)

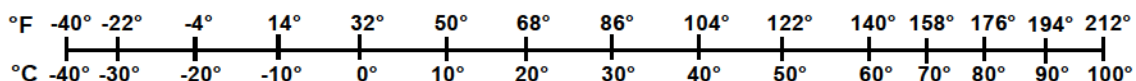|		
1 milliliter (ml)	=	0.03 fluid ounce (fl oz)
1 liter (l)	=	2.1 pints (pt)
1 liter (l)	=	1.06 quarts (qt)
1 liter (l)	=	0.26 gallon (gal)
1 cubic meter (m³)	=	36 cubic feet (cu ft, ft³)
1 cubic meter (m³)	=	1.3 cubic yards (cu yd, yd³)

TEMPERATURE (EXACT)

$[(9/5)\ y + 32]\ °C = x\ °F$

QUICK INCH - CENTIMETER LENGTH CONVERSION

Inches	0	1	2	3	4	5
Centimeters	0	1 2 3	4 5	6 7	8 9 10	11 12 13

QUICK FAHRENHEIT - CELSIUS TEMPERATURE CONVERSIO

°F	-40°	-22°	-4°	14°	32°	50°	68°	86°	104°	122°	140°	158°	176°	194°	212°
°C	-40°	-30°	-20°	-10°	0°	10°	20°	30°	40°	50°	60°	70°	80°	90°	100°

For more exact and or other conversion factors, see NIST Miscellaneous Publication 286, Units of Weights and Measures. Price $2.50 SD Catalog No. C13 10286

Acknowledgments

Contents

Illustrations

vii

Tables

Executive Summary

The Volpe Center (Volpe) and the Federal Railroad Administration (FRA) are engaged in active research aimed at improving rail vehicle crashworthiness. One component of this research is focused on improving the performance of passenger train cab cars during collisions with heavy objects at grade crossings. Standards were approved by the American Public Transportation Association (APTA) on October 14, 1999 and later revised (Revision 1 Approved May 22, 2003; Revision 2 Approved April 10, 2006) [1]. These standards increase the strength requirements for cab car end structures and impose further requirements on their ability to absorb energy during a collision. FRA issued a Notice of Proposed Rulemaking on August 1, 2007 to include these new standards in 49 CFR §238.211 [2].

To aid in the development of these standards, FRA and Volpe conducted a set of three tests: quasi-static loading of both the collision and corner posts and dynamic loading of the collision post only. (A dynamic test of the corner post was conducted as part of an earlier program.) Volpe developed these tests to illustrate testing methodologies and to demonstrate the feasibility of the new energy absorption and large deformation requirements in the APTA standard and in Federal regulations.

In support of this testing program, the primary objective of the work described here was to adapt the state-of-the-art (SOA) end frame design originally built for retrofit onto the Budd Pioneer car so that it could be retrofit onto a Budd M1 car. With the aim of using a single cab car for all three tests, the M1 car was reinforced so that it would be strong enough to support the loads that would be transmitted to the end structure during the tests. Volpe designed the connections between the end frame and the car body so that they could be easily cut away from the car body after each test so that a new end frame could be connected. Finally, the end frame design was modified to account for differences between the M1 and Budd cab car designs.

With these objectives in mind, Volpe developed a design for the retrofit. The associated computer-aided design model was used as a basis for a set of detailed design drawings and for the construction of a finite element model of the car. The design drawings were, in turn, used to fabricate the required steel components for three complete sets of end frames, three sets of end frame-to-car body connections, and a single set of car body reinforcements.

Volpe then developed a finite element (FE) model of the end frame retrofit onto the M1 cab car based on the detailed design. A series of linear and nonlinear static, quasi-static, and dynamic finite element analyses were conducted to guide the design of the end frame retrofit onto an existing cab car, determine if the design satisfied the structural requirements imposed by the new rules, and predict the outcome of the recent full-scale tests.

Preliminary analyses revealed the need for a few minor modifications to the connections in order to meet design requirements; these were incorporated into the final design for manufacture.

Components for the end frame, connections between the end frame and the car body, and reinforcements to the car body were fabricated based on detailed design drawings and then assembled and connected to the reinforced M1 car, from which the original end frame had been cut off.

Zimmerman Metals in Denver, Colorado, fabricated the parts and delivered them to the Transportation Technology Center in Pueblo, Colorado. Transportation Technology Center, Inc., under separate contract to FRA, prepared the M1 car body for retrofit, attached the car body reinforcements, assembled each end frame, and attached it to the reinforced car using the fabricated connector elements. After each of the first two tests, the damaged end frame and connector elements were cut off and a new set was attached.

With the knowledge that material failure was observed in the 2002 corner post impact test, a material failure model based on the Bao-Wierzbicki criterion [3] was incorporated into the FE models to improve the accuracy of model predictions. Following a set of preliminary calculations to assess the effect of element type, mesh refinement, etc., on the failure behavior of an impacted post, the material failure model was successfully implemented into the FE model of the SOA end frame and validated through analysis of the 2002 impact test.

Volpe then used the validated model to predict the outcome of the dynamic impact test (conducted in April 2008). The results of model predictions were compared with test results. While there was a reasonable level of agreement between the model predictions and the outcome of the test, some aspects of the test were not well-captured by the model. Model parameters were modified based on this comparison and the model was subsequently used to predict the outcome of the quasi-static collision post load test (June 2008). Agreement between model predictions and test results was lacking for this test. An extensive analysis of the test results and a series of post-test experiments ultimately revealed a design feature that adversely affected the ability of the post to deform, but was not captured by the model. The design of the end frame was modified based on this investigation.

Finally, Volpe used the revised model to predict the outcome of the quasi-static corner post load test (August 2008), which was conducted using the modified end frame design. The predictions of this model were in excellent agreement with the results of the test, both in terms of the modes of deformation and fracture and the resulting force-displacement and energy-displacement characteristics.

1. Introduction

The Volpe Center supports the analysis and full-scale testing program of the Federal Railroad Administration (FRA) directed at understanding and improving rail vehicle crashworthiness. The objectives of this testing program are to establish the crashworthiness of vehicles built to current standards and to assess the improvements provided by new requirements and new technologies. The testing program has been focused on two general types of accident scenarios: collisions between two rail vehicles and grade-crossing collisions. Investigation into each of these broad classes has spawned a comprehensive series of full-scale tests.

1.1 Background

In collisions between two rail vehicles, the underframes of the vehicles most often bear the brunt of the collision load, and research in this area has generally been focused on improvements to the design of underframe structures at the ends of the cars. In grade-crossing collisions, the vehicle is often loaded above the underframe, where it is weaker. Research in this area has been focused on improving the strength of vehicle end structures that are above the underframe. This is particularly true for cab cars, which are not as strong as locomotives, and where cab occupants are positioned very close to the leading end of these vehicles.

Cab cars are passenger-carrying rail vehicles located at one end of the train with a locomotive on the other to provide tractive effort. The cab car becomes the lead car when the train is operated in the push-mode, with the locomotive pushing the train. The operator is positioned at the front end of the cab car where he or she has good visibility of the track. In the U.S., the cab car is designed to also be used as a passenger car within the train. This requires that the cab car have the same layout as a coach-style passenger car, with the result that the operator is located immediately adjacent to the forward flat end wall of the vehicle. Figure 1 shows an example of a cab car operated in the U.S. The end wall includes two collision posts, one on each side of a doorway, and posts at each corner. Despite these safety features, the proximity of the operator to the very end of the car puts him or her at greater risk in the event of a collision with an object or another train.

Figure 1. An example of a cab car in which the operator is positioned immediately adjacent to the vehicle end

To increase the safety of passenger train occupants, FRA, through a Notice of Proposed Rulemaking (NPRM), proposed amendments to regulations governing the structural behavior of the front end of cab cars and multiple-unit locomotives [2]. In addition to numerous requirements for the strength of key end frame components, the proposed regulations impose requirements for energy absorption and post deformation, following recommendations of the American Public Transportation Association (APTA) [1].

The proposed rule provides two alternative testing methods for demonstrating absorption of collision energy. Following the quasi-static method, the front end structures must be capable of absorbing a specific amount of energy – 135,000 ft-lbf for a load applied to the collision post and 120,000 ft-lbf for a load applied to the corner post. Following the dynamic method, the structure must be capable of withstanding a longitudinal impact of a proxy object that imparts approximately the same amount of collision energy to each post, respectively. For example, for a 14,000-lbm proxy object impacting a 70,000-lbm vehicle, the impact speed must be at least 18.2 mph for the collision post test or 17.1 mph for the corner post test to impart the required amount of collision energy.

In both the quasi-static and dynamic test scenarios, the load is applied approximately 30 inches above the underframe. No more than 10 inches of longitudinal permanent deformation into the occupied volume is allowed. Some fracture is permitted, as long as the post does not completely separate from the end frame.

In an earlier program conducted by the Volpe Center and sponsored by FRA [4], a design was developed for a cab car end frame that satisfies Federal regulations that were introduced in 1999. This so-called state-of-the-art (SOA) end frame was fabricated and retrofit onto Budd Pioneer cab cars that were donated for testing.

A coil impact test of the corner post of the SOA end frame (replicating the scenario in the dynamic option permitted by the new rule) was conducted at FRA's Transportation Technology Center (TTC) in June 2002. The results of the test indicated that the SOA end frame was a substantial improvement to a design built to pre-1999 Federal regulations (the "1990s design") [5]. The corner post of the SOA end frame deflected about 9 inches due to impact by a 40,000 lbm, 6-ft-diameter by 4-ft-wide steel coil traveling at 14 mph, with the post fracturing in a few locations, but remaining attached to the end frame. In contrast, in the corresponding test of the 1990s design, the impact of the coil caused the corner post to completely separate from the end frame, displacing the full extent of the operator cab volume (a distance of about 3 feet).

To help evaluate the proposed rules and test methods described above, the Volpe Center conducted three additional tests of the SOA end frame. A dynamic impact test of the collision post was conducted in April 2008 [6, 7]. A quasi-static test in which the end frame was loaded at a collision post was conducted in June 2008. A quasi-static test with the load applied to the corner post was conducted in August 2008 [7]. The work described in this report was conducted in support of this testing program.

1.2 Objectives

Budd Pioneer cars were not available for use in this testing program; instead, Budd M1 cars were utilized. The primary objective of the program described here was to adapt the SOA end frame design originally built for retrofit onto the Budd Pioneer car so that it could be retrofit onto a Budd M1 car. With the aim of using a single cab car for all three tests, the M1 car was reinforced so that it would be strong enough to support the loads that would be transmitted to the end structure during the tests. Connections between the end frame and the car body were designed so that they could be easily cut away from the car body after each test so that a new end frame could be connected. Finally, the end frame design was modified to account for differences between the M1 and Budd cab car designs.

1.3 Overall Approach

With these objectives in mind, Volpe developed a design for the retrofit. The associated computer-aided design (CAD) model was used as a basis for a set of detailed design drawings and for the construction of a finite element (FE) model of the car. The design drawings were, in turn, used to fabricate the required steel components for three complete sets of end frames, three sets of end frame-to-car body connections, and a single set of car body reinforcements.

Zimmerman Metals in Denver, Colorado, fabricated the parts and delivered them to TTC in Pueblo, Colorado. TTCI, under separate contract to FRA, prepared the M1 car body for retrofit, attached the car body reinforcements, assembled each end frame, and attached it to the reinforced car using the fabricated connector elements. After each of the first two tests, the damaged end frame and connector elements were cut off and a new set was attached.

Finite element analyses (FEAs) were used to guided the design of the end frame retrofit onto an existing cab car, determine if the design satisfied the structural requirements imposed by the new

rules, and predict the outcome of the recent full-scale tests. With the knowledge that material failure was observed in the 2002 corner post impact test, a material failure model was incorporated into the FE models with the aim of improving the accuracy of model predictions.

1.4   Scope

This report details the design of the retrofit of an M1 car with a SOA end frame and the fabrication and assembly of the end frame onto an M1 cab car. FEAs were conducted and three full-scale tests were performed on the retrofit M1 car. The test results are compared with the analyses and conclusions are provided.

1.5   Organization of the Report

The report is arranged as follows:

Section 2 describes the requirements for the design for the end frame retrofit.

Section 3 discusses the development of the design of the retrofit, including preparation of the M1 car, reinforcement, and modifications.

Section 4 details the fabrication of the components, the preparation of the M1 for retrofit, and the assembly of the retrofit, including quality control measures used during the fabrication and assembly process.

Section 5 contains the analysis of the design, including static, quasi-static, and dynamic analyses, as well as the predicted energy absorption and the development of a material failure model.

Section 6 provides a brief summary of the report and conclusions drawn from the analyses and tests.

2. Requirements

The primary structural requirements for the design of the end frame and supporting structures were derived from the FRA NPRM and the APTA standard. A specifications document was generated as part of the design process to provide guidance for generating concepts and quantitative measures for evaluating the design. This document is attached to this report as Appendix A.

2.1 Structural Requirements

The structural requirements can be separated into two categories: strength requirements and energy absorption requirements. The strength requirements are unchanged from those that were used to design the SOA end frame for retrofit onto the Budd Pioneer cab car and are summarized in Figure 2 and Table 1. Most of these are based on a yield strength criterion, i.e., when the load is applied, there can be no yielding of the end frame or its supporting structures. The 200,000-lbf longitudinal load on the collision post at 30 above the underframe and the 500,000-lbf longitudinal load on the buffer beam are based on an ultimate strength criterion.
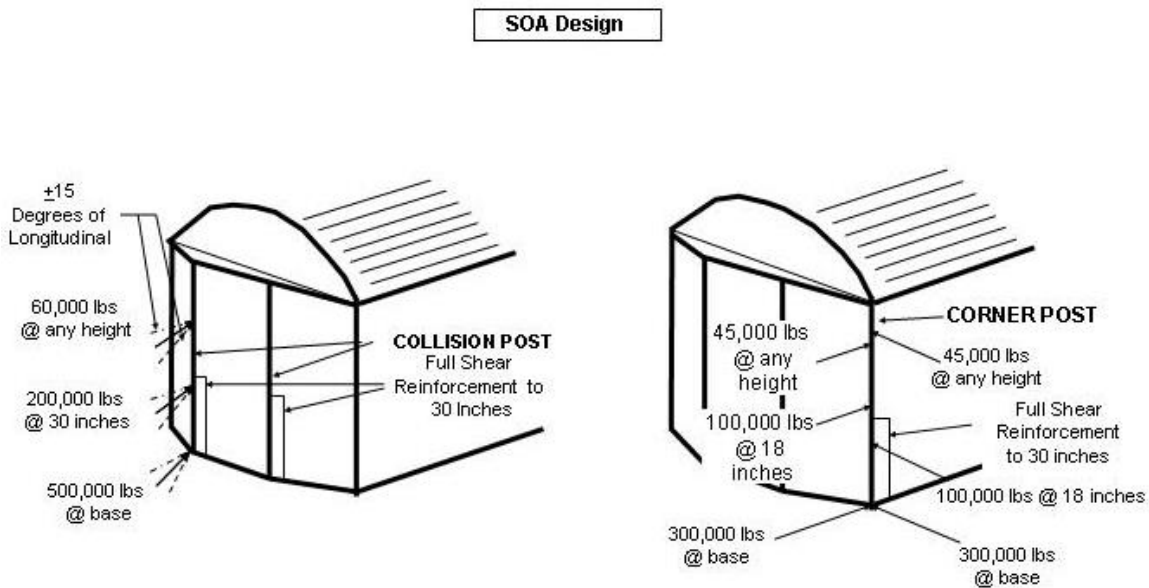
Figure 2. Illustration of some of the structural requirements for the SOA design

Table 1. Summary of cab car end structure crashworthiness standards and requirements

Component	Requirement
Collision Post (must be present at the 1/3 points along the width of the vehicle)	• 500,000 lbf (2224 kN) at the floor without exceeding the ultimate shear strength • 200,000 lbf (890 kN) at 30 inches (762 mm) without exceeding the ultimate strength • 60,000 lbf (267 kN) applied anywhere without yield. • All requirements apply for loads applied ±15° inward from the longitudinal. • Strengths must be achieved without failing connections. • The post must be able to deform substantially without failing the connections.
Corner Post (must be present at the extreme corners of the vehicle)	• 300,000 lbf (1344 kN) at the floor without exceeding the ultimate shear strength • 100,000 lbf (445 kN) at 18 inches (460 mm) above the floor without exceeding the yield strength • 45,000 lbf (200 kN) applied anywhere along the post without yield. • All requirements apply for loads applied anywhere between longitudinal inward to transverse inward.
Lateral Member (must be present between the corner and collision posts just below the cab window)	• 15,000 lbf (66.7 kN) applied in the longitudinal direction anywhere between the corner and collision post without yield. • Include a bulkhead in the opening below the shelf.

2.2 Other Requirements

In addition to the crashworthiness requirements, it was also important to ensure that the designs were practical with regard to other operational and physical requirements. These requirements include accommodation for conventional coupling components and restricting dimensions to fit into standard vehicle clearance envelopes.

3. Design Development

Several differences between the Pioneer car and the M1 car, both geometrical and structural, were addressed in developing the design. The car body profiles are different, with the M1 car having a more rounded cross-section. There are also significant differences in floor height that had to be accounted for. For the most part, the design of the adaptation of the SOA end frame to the M1 car can be categorized as having four components:

- Preparation of the M1 car

- Reinforcement of the structure on the M1 car so that it can withstand the higher loads associated with the SOA end frame requirements for multiple tests.

- Addition of connections between the post-cut M1 car and the SOA end frame

- Modification of the end frame to account for geometrical and structural differences between the Pioneer and M1 cars.

3.1 Preparing the M1 Car for Retrofit

The end of the existing M1 car was cut off at appropriate locations to accommodate the required connections to the SOA end frame. A single planar cut was made around most of the side and roof structure of the car body. A more complex 3-dimensional cut was made around the forward end of the draft sill. Figure 3 shows a CAD representation of the cut M1 car.
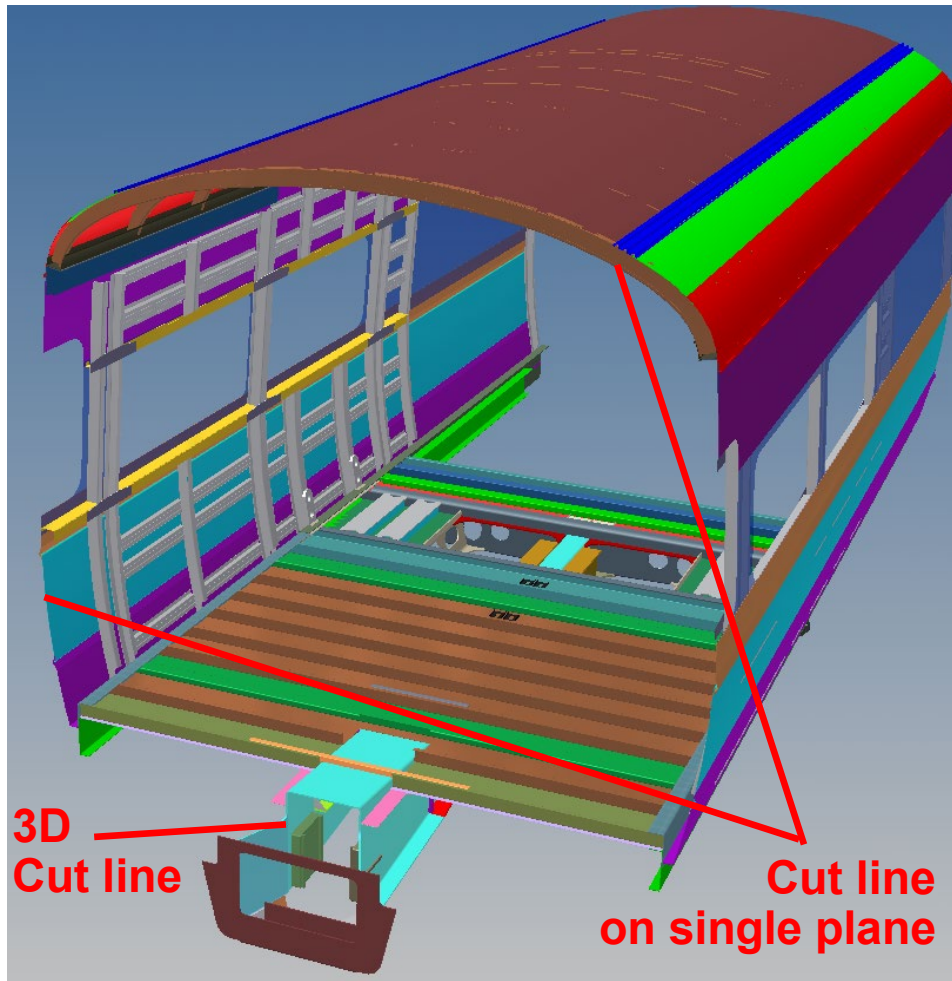
Figure 3. CAD representation of the car cut line

3.2   Car Reinforcement

Reinforcements were added to the M1 car body to ensure minimal damage to the existing car structure during each test. The sideframe posts were shortened and 0.188-inch doubling plates were mechanically fastened to the bottom of the roof rail and on the side directly below the existing rail, as shown in Figure 4. The doubling plates were used to provide mechanical fastening to the original stainless steel sideframe. In addition, a 0.25-inch-thick tube was welded directly below the existing roof rail to provide an interface with the connections to the end frame, and was attached to the posts with brackets to restore torsional fixity of the top of the original posts, as shown in Figure 5.
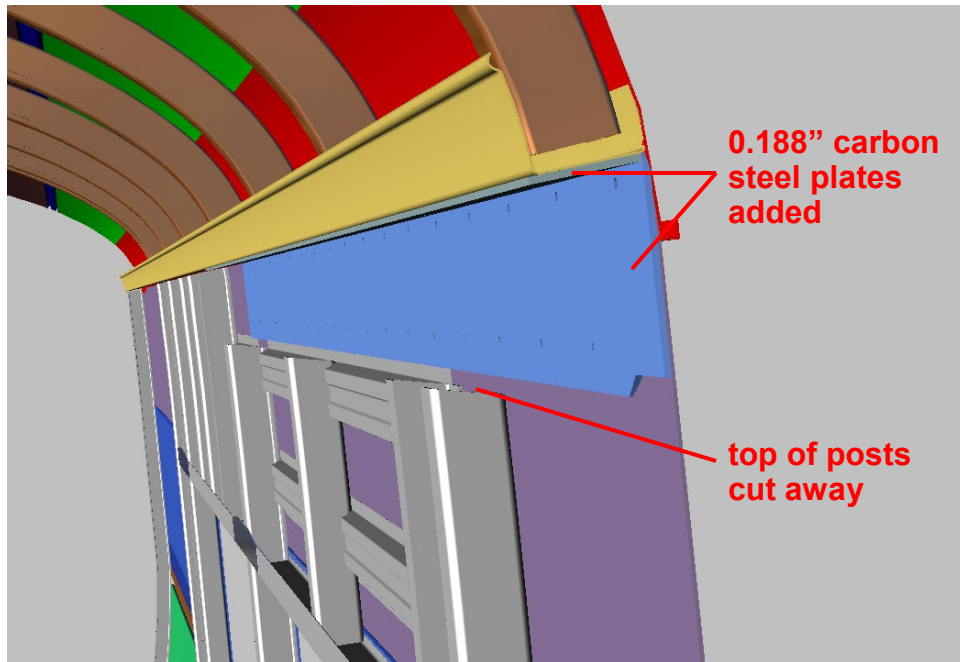
Figure 4. Reinforcement plates fastened to side wall and roof rail
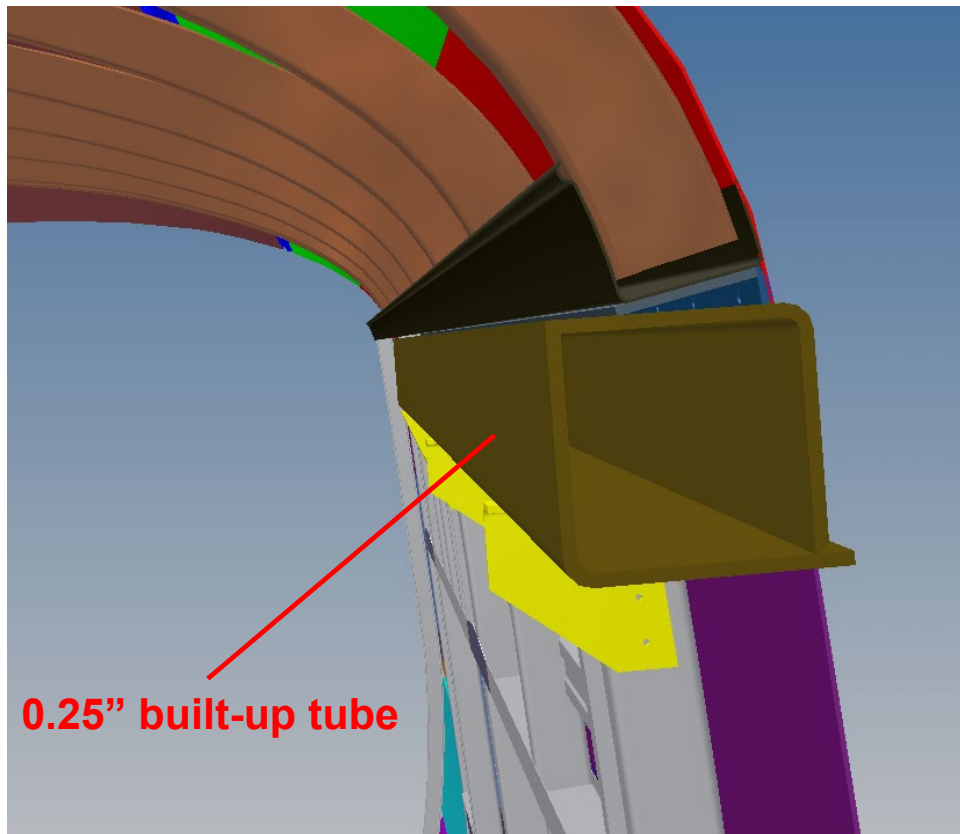
Figure 5. Built-up tube welded to doublers for longitudinal load path into roof rail

Reinforcement plates, 0.188-inch thick, were mechanically fastened to the side sill to form a box structure. Above the floor pans, an open channel was mechanically fastened to the top of the side sill. These modifications are shown in Figure 6.
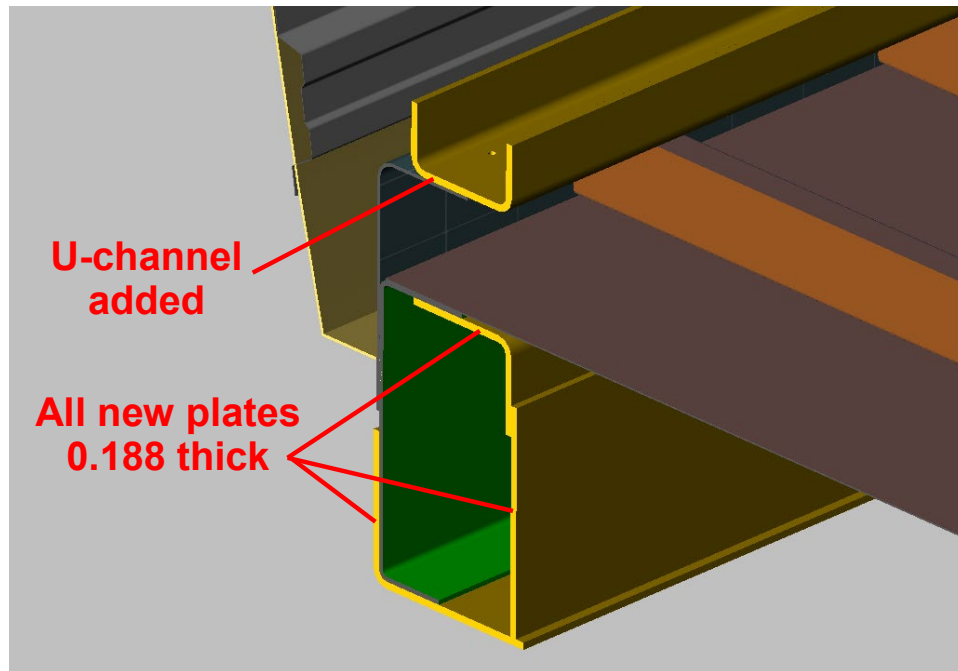
Figure 6. Side sill reinforcements for M1 car

A triangular bracing structure, shown in Figure 7, was added to fulfill part of the structural function of the side and end sheets that were removed. The brace added racking stability to the end of the car and vertical restraint to the center sill without affecting its crush strength.
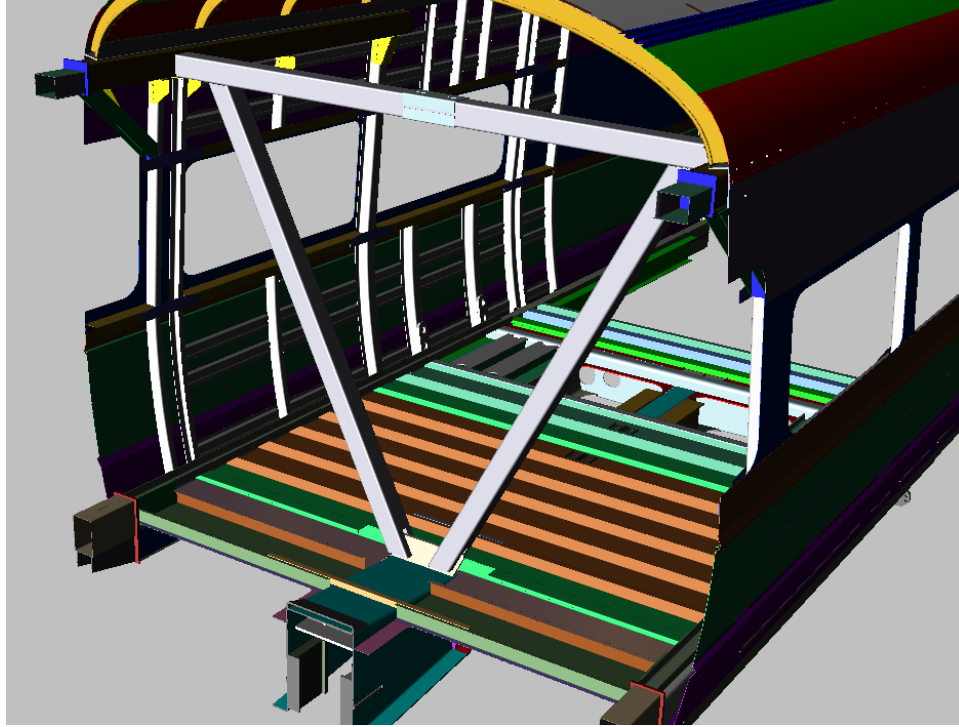
Figure 7. Triangular bracing structure

3.3   Connections to the End Frame

There are five connection points between the car body and the end frame – one at the center sill, two at the side sills, and two at the roof rails. Each of these connections was redesigned for the retrofit.

The connection of the roof rail to the end frame included a 0.179-inch-thick tube with a rectangular cross-section tapering along its inside edge, as shown in Figure 8. The tube was capped on either end with 0.5-inch-thick plates to distribute the bearing load over the anti-telescoping (AT) beam and roof rail tube, respectively.

At the side sill, the connection included two 0.134-inch-thick C-channels forming a rectangular tube on top, and two 0.188-inch-thick tapered plates providing the transition in height from the bottom of the side sill to the bottom of the end beam, as illustrated in Figure 9. The tube was closed at both ends with 0.5-inch plates to distribute the bearing loads.

0.5" thick end plates

0.179" thick built-up tube
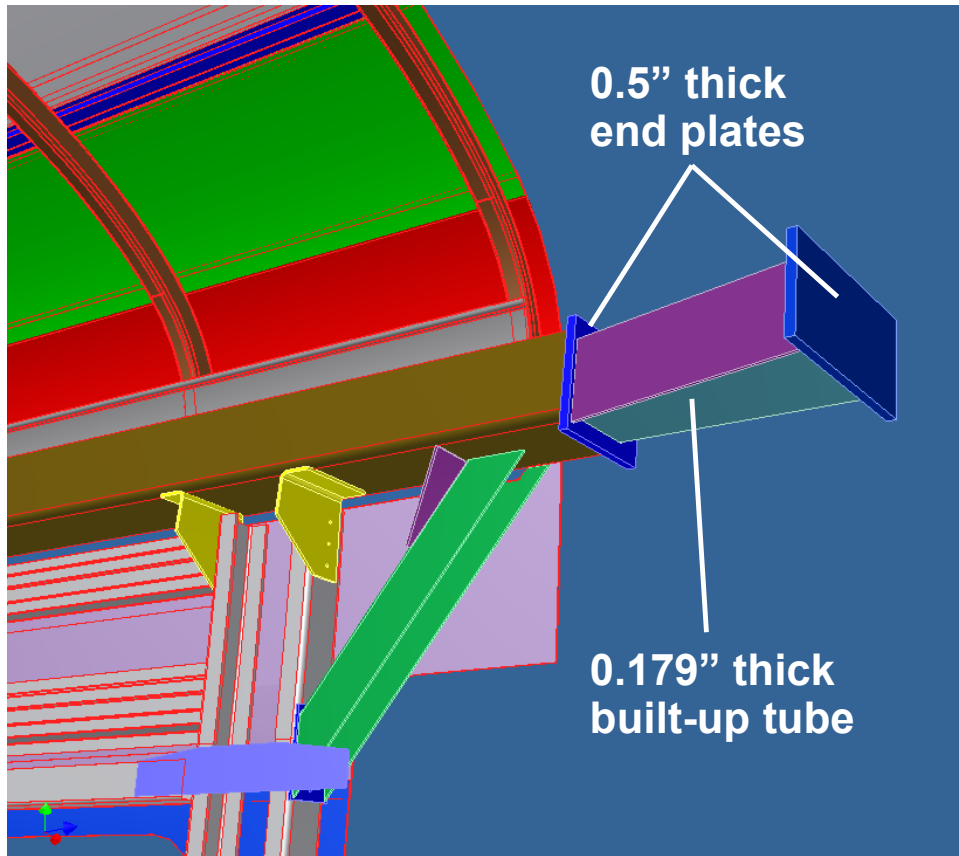
Figure 8. Roof rail connections
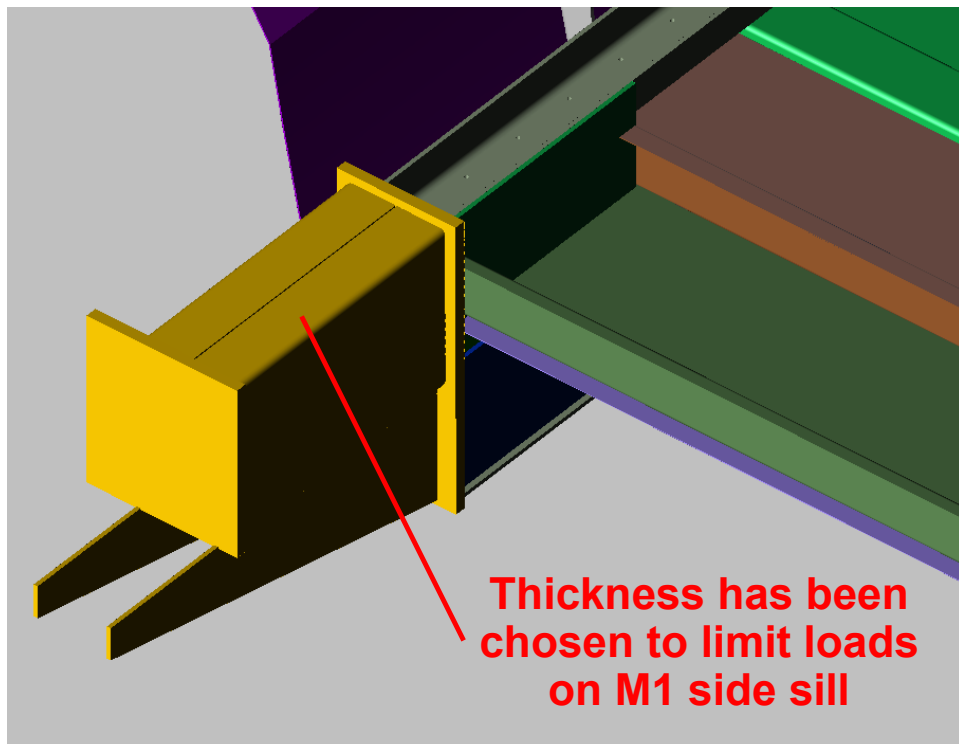
Thickness has been chosen to limit loads on M1 side sill

Figure 9. Side sill connections

The connection at the center sill was similar to that of the SOA design for a Pioneer car. However, because there is a height difference between the Pioneer and M1 cars, components were added above and below the top flange of the center sill, as shown in Figure 10. In addition, the bell mouth was extended to accommodate the deeper SOA end beam.

Bellmouth web extension

Angled portion added for continuity with end beam top
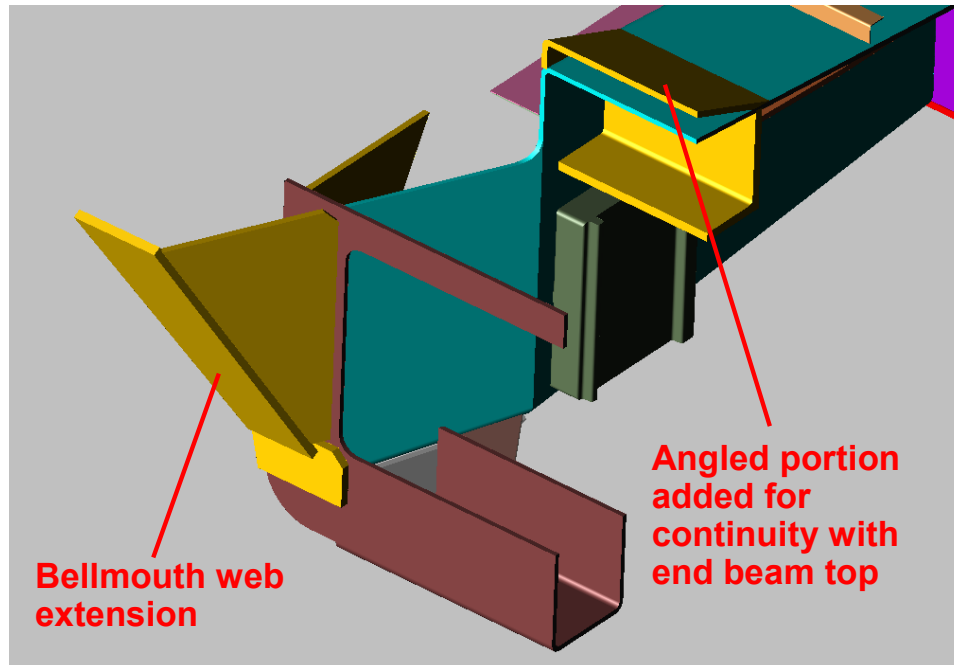
Figure 10. Cross-sectional view of the center sill with transitional structure for M1 car

3.4 Modifications to the End Frame

The design of the SOA end frame itself required only a few modifications to adapt to the M1 car body. Due to the rounded shape of the M1 car body as compared to the Pioneer cab body, the lateral extent of the AT beam was changed slightly so that it extended beyond the corner post by 1.5 inches, as compared to 1.0 inch for the Pioneer Car. Figure 11 shows the SOA end frame with the bulkhead, AT beam, and buffer beam cover plates removed so that the reinforcing gusset plates can be viewed. The complete car model is shown in Figure 12.
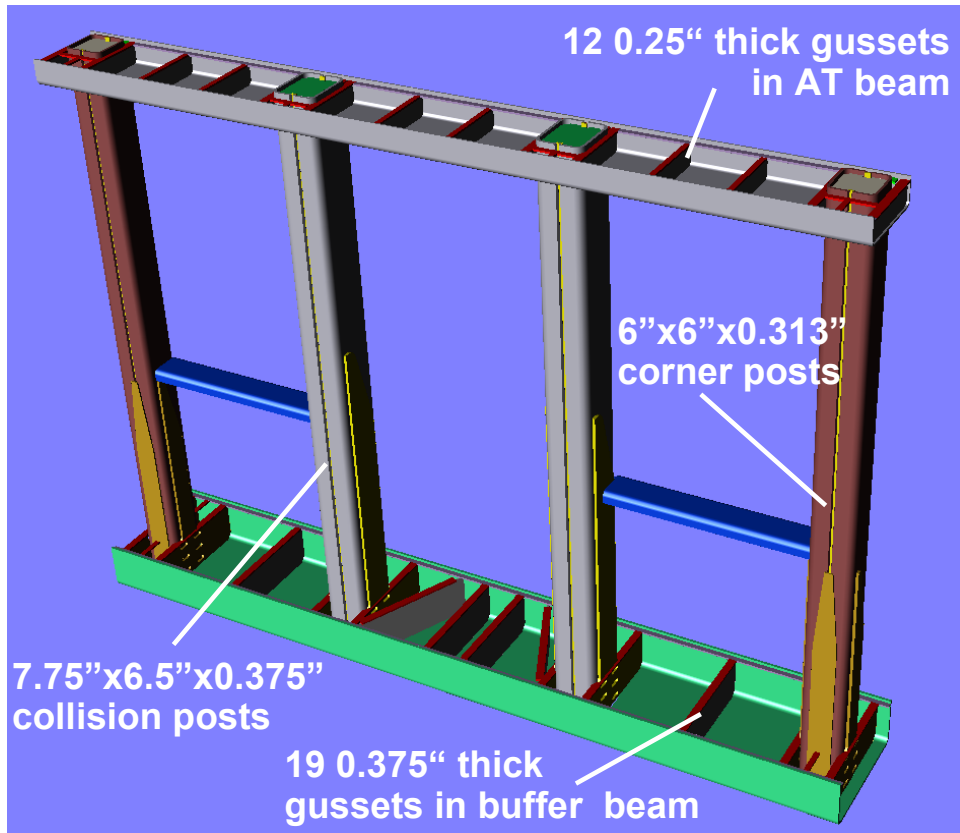
Figure 11. The end frame with the bulkhead, AT beam, and buffer beam cover plates removed
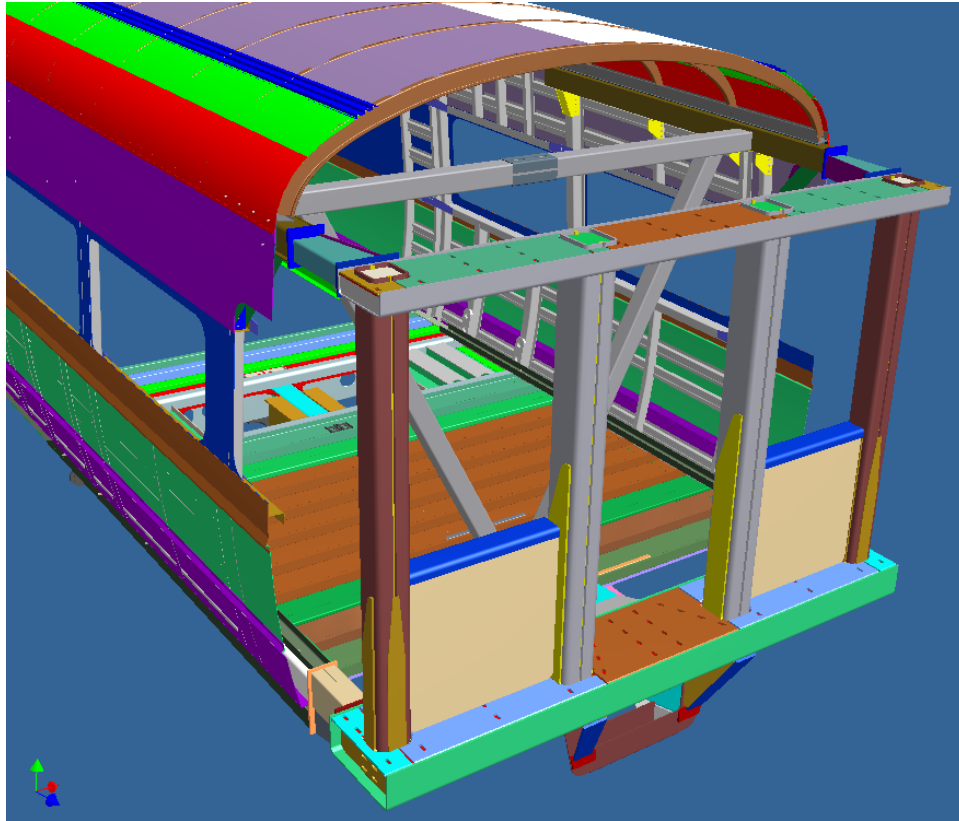
Figure 12. The complete CAD model for the M1 car with SOA end frame

3.5   Detailed Design Drawings

Using the CAD model, a complete set of detailed design drawings was created. The drawing package included:

- Cut drawings – specifying how the M1 car should be cut so that the new end frame can be installed.

- Fabrication drawings – specifying how the individual components for the end frame, the end frame-to-car body connections, and the car reinforcement parts should be fabricated.

- Installation drawings – specifying the procedure for installing the individual fabricated components for the end frame, the end frame-to-car body connections, and the car reinforcement parts on the prepared M1 car body.

In addition to the detailed drawings, TRA Inc. also supplied to TTCI a PowerPoint document that provides direction as to the proper sequence of component installation.

Appendix B contains the list of detailed drawings created.

3.6   Design Modifications

The initial design for the SOA end frame/M1 retrofit was modified twice during the program. Two modifications were made as a result of preliminary analysis work. A triangular gusset was added at the connection between the draft sill and the back of the buffer beam to relieve a stress concentration that was identified in preliminary analyses (see Figure 13). In addition, the

17

thickness of the roof-rail connection tube was increased from 0.134 inch to 0.188 inch (see Figure 8).

Another modification was made following the quasi-static collision post-test. The depth of the shelf was decreased and straps tying the back of the shelf to the corner and collision posts were removed. This change is described in Section 5.3.
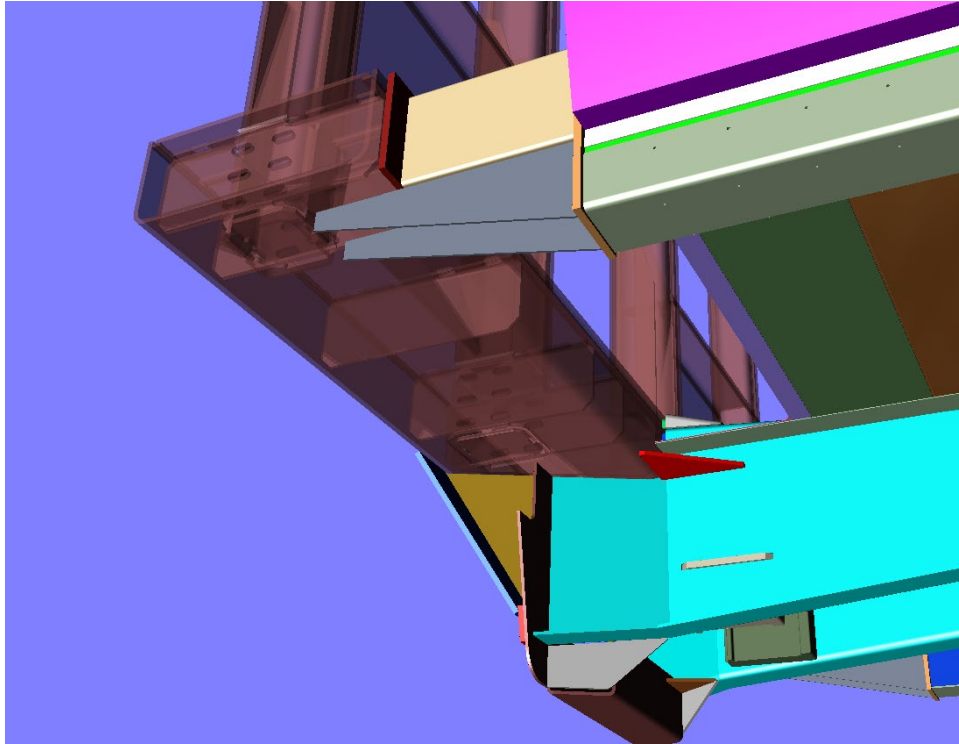
Figure 13. View from below the underframe of CAD model for M1 Car with SOA endframe, with triangular gusset plate shown in red

4. Fabrication and Assembly

The many components that make up the SOA end frame, plus the car body reinforcements and the end frame-to-car body connection elements, were fabricated based on the detailed drawings created from the CAD model. A single set of reinforcement parts was fabricated with the intention of re-using them for all of the tests. Three complete sets of connection and end frame parts were made, one for each of the tests. Approximately 670 parts were fabricated from various carbon steels, each with a minimum specified yield strength of 50 ksi.

4.1 Component Fabrication

All the individual components were fabricated from plate steel at Zimmerman Metals in Denver, Colorado. The fabrication process consisted primarily of laser cutting the steel plates, beveling edges, and bending the plates using large brake presses.

4.1.1 Materials

Originally, the entire end frame was designed to be constructed from A710 Grade A, Class 3 steel, as this steel had been used to fabricate the SOA end frame in previous programs. Unfortunately, this material was in extremely high demand due to its heavy use by the military. Instead, a mix of other steels that were available from Zimmerman's suppliers was selected — specifically, A572-50 and A656-80. The key mechanical properties for these steels are compared with those of A710 in Table 2.

Table 2. Comparison of A572-50 and A656-80 steel mechanical properties procured for fabrication of the SOA end frame with those of A710 steel

Plate Thickness (in)	Material	Yield Strength (ksi)	Ultimate Strength (ksi)	Elongation (%)
0.25–0.5	A710	80*	85*	20% in 2" *
0.25	A656-80†	81–93	99–93	20–24% in 2"
0.312	A656-80†	82	101	20% in 2"
0.375	A572-50†	64	78	20–21% in 8"
0.5	A572-50†	66–72	78–82	30–33% in 2"

* per specification
† per material data report

Note that the A710 properties listed in Table 2 represent minimum specified values, whereas the A572-50 and A656-80 properties are based on measurements made on the actual lots of steel used for fabrication, as provided in material test reports. The properties of A656-80 are quite similar to those of A710, as they are both high-strength, low alloy steels, with a minimum specified yield strength of 80 ksi. The minimum specified yield strength of A572-50 is only 50 ksi; however, as with most steels, its actual measured strength is considerably higher. In this case, the weaker of the two A572-50 steels exhibited a measured yield strength about 20 percent lower than the minimum specified yield strength of A710, and a measured ultimate strength that was only about 10 percent lower.

Prior to procurement of the components, FEA models were used to demonstrate that all the structural requirements could be met using the alternative steels. Note that the collision post was constructed primarily from 0.375-inch-thick plates and reinforced with 0.375-inch-thick gussets – so it consisted almost entirely of A572-50. On the other hand, the corner post was constructed primarily from 0.312-inch-thick plates and reinforced with 0.25-inch-thick gussets – so it consisted almost entirely of A656-80. Likewise, the buffer beam was mostly constructed of 0.375-inch-thick plates and therefore consisted mostly of A572-50, while the AT plate was primarily constructed from 0.25-inch material and therefore consisted mostly of A656-80.

4.1.2 Quality Assurance

A quality assurance activity was performed to ensure the fabricated parts were cut and formed according to drawing specifications, properly labeled, and delivered to TTC. A quality control document was created for this purpose and is included in Appendix C. It addresses the quality control requirements for the materials supplied by and components fabricated by Zimmerman Metals as well as the welding and assembly conducted at TTC.

Inspection of most of the fabricated parts was conducted at Zimmerman's facilities in February and March 2008. A large spreadsheet-based checklist for all of the parts was created and used for this purpose.

An initial batch of parts that were necessary for use in the early stages of the M1 car reinforcement process was inspected and picked up by TTCI in February. Most of the remaining parts were inspected during a site visit to Zimmerman in March 2008 by TIAX personnel. This visit revealed the following:

- Several parts were not labeled or were incorrectly labeled. These deficiencies were corrected on-site.

- One of six backing angles used for car body reinforcement (part no. D038-009-032) was found to have a crack in it. This part was later re-fabricated by Zimmerman and delivered to TTCI.

- Two sets of end frame component parts were found to have had the beveling done on the wrong side of the part (part no. D038-009-010 #42 – buffer beam top plate right-hand, and part no. D038-009-010 #44 – AT plate top plate right-hand). These parts were also re-fabricated and delivered to TTCI.

- The slots in the two diagonal brace components were cut a little too large (just over 1.0 inch versus the 0.875-inch specified dimension). It was deemed that this dimension was not critical and that filler material could be added during welding of the brace to the brace connection gusset.

- A mistake was found in a dimension listed on the drawing for the roof rail brace (part no. D038-009-018). This error was subsequently corrected.

- A few of the larger parts had not yet been formed at the time of the inspection visit due to a problem with the large brake press. These parts were formed a few days later and delivered to TTCI, where they were inspected. One of these parts, the large C-channel that forms the bottom, front and back sides of the buffer beam (part no D038-009-010 item #2), was found to have a crack running along one of the bends (see Figure 14). This part was rejected. Zimmerman re-fabricated this part with one that was later deemed to be acceptable.

Figure 14. Photograph of cracked buffer beam channel that was rejected and re-fabricated

4.2   M1 Car Preparation

The original end of the M1 Car was cut off according to drawings provided for this purpose. Figure 15 shows a photograph of the cut M1 car prior to adding the reinforcing structure.

Figure 15. The cut M1 car ready for retrofit

There were several issues that were addressed as the M1 car was prepared, including the following:

- This car had been in an accident and was damaged. As is evident in Figure 15, the left side of the car was missing much of its skin. There was some concern that this might affect the strength of the car body. It was decided that all of the loads would be applied on the other side of the car to limit the forces transmitted through to this side of the car. In addition, an FE analysis was performed with the skin removed that showed that there was sufficient strength even without the skin.

- There was some unevenness in the floor near the side sill in a region that was to be reinforced with an additional plate fastened with huck bolts. Shims were placed between the floor and the reinforcement plate to close the gaps. The shims were tack-welded to the new plate prior to huck bolting.

- The center sill bottom flange was damaged and susceptible to buckling. It was agreed that this flange would be in tension during the tests and not sensitive to this damage. No action was taken to repair the damage.

- The bell-mouth on the car was not consistent with drawings. The faceplate was damaged and appeared to have had a homemade striker plate welded to it. The face plate was cut off and replaced with a new one.

- The part of the buffer beam that was originally on the car extended 21 inches from the end of the car, not 16 inches like the new buffer beam. It was confirmed that this beam should be cut at 16inches.

4.3   Assembly

The end frame was assembled and then attached to the cut M1 car. A few minor issues arose during the assembly, including the following:

- The bulk head plate (D038-009-010 item #65) that fits between the shelf, the buffer beam, and the collision and corner posts was found to be ⅜-inch short at the top edge. A change was made to have the plate butt against the bottom edge of the inside shelf flange, with a full penetration weld and backing bar at this connection, replacing the double fillet weld that was specified in the assembly drawing. All other welds to the plate remained as specified.

- A problem was encountered with detailing for the outside backing bar (D038-009-010 item #51) on the AT beam top plate (D038-009-010 item #45). The fabrication detail for item #51 calls for a cope (a cut-out) of the inside backing bar so that it fits along the inside of the corner post. The fabrication detail for the backing bar on the outside of the corner post did not, however, call for a cope, as it should have. If the backing bar is also coped on the outside to provide a good fit around the corner post, the slot for the plug weld in the top plate is partially open on the outside of the backing bar. This problem was corrected for the first end frame by placing a fillet weld underneath the top plate, along the outside edge of the backing bar, to fill the gap and reinforce the plug weld area of influence. The drawing was corrected so that the outside backing bar was coped. It was widened from 1.125 inches to 2.0 inches so that the plug weld slot would be fully closed

A photograph of the assembled end frame installed on the M1 car prior to the dynamic coil impact test is shown in Figure 16.

Figure 16. SOA end frame integrated with M1 car

5. Design Analysis

FEA was used to evaluate the M1 cab car/SOA end frame design. To demonstrate compliance with structural requirements, a comprehensive set of analyses were performed:

- Linear and nonlinear static analyses
- Large-deformation quasi-static analyses
- Large-deformation dynamic impact analyses

An FE model of the forward half of the cab car was developed to evaluate the design against static load requirements. This model was also used to conduct preliminary calculations, evaluating the performance of the design against requirements for quasi-static loading and dynamic impact of the collision and corner posts.

The 3-dimensional CAD model, shown in Figure 12, was used not only as the basis for the detailed drawings that guided the fabrication of components but also as the starting point for building FE models of the SOA end frame/M1 cab car retrofit. Detailed models of the car were constructed using the Hypermesh program [8]. Both full-width and half-width models of the forward half of the car (i.e., half-car and quarter-car models) were built. Figure 17 shows the mesh constructed for the full-width model. This model uses roughly 160,000 elements, most of which are shells. The rest are beam elements which are only used in the middle of the car, far from the region of high deformation. Note that, due to the high level of mesh refinement, element outlines are not indicated in this figure. The mesh is most refined near the front of the car, with a characteristic element length of approximately 1 inch.

Partway through the analysis effort, the scope of the modeling component of the program was expanded to include the development and implementation of a material failure model. Capturing material failure required much more mesh refinement in the regions of the end frame that experienced the high levels of strain that are associated with material failure. For this reason, a model of only the end frame and its connections was developed and used to simulate the quasi-static and dynamic tests, as shown in Figure 18. Use of the limited-extent submodel was possible because one of the fundamental goals of the design was to limit permanent deformation to only the end frame and connector components so that the reinforced car body would be undamaged and re-usable for subsequent tests. Supplemental analyses were performed to demonstrate that the results of analyses were not significantly altered when the less extensive, but more refined, model was used. A comparison of the predicted force-displacement curves from these supplemental analyses is also shown in Figure 19.
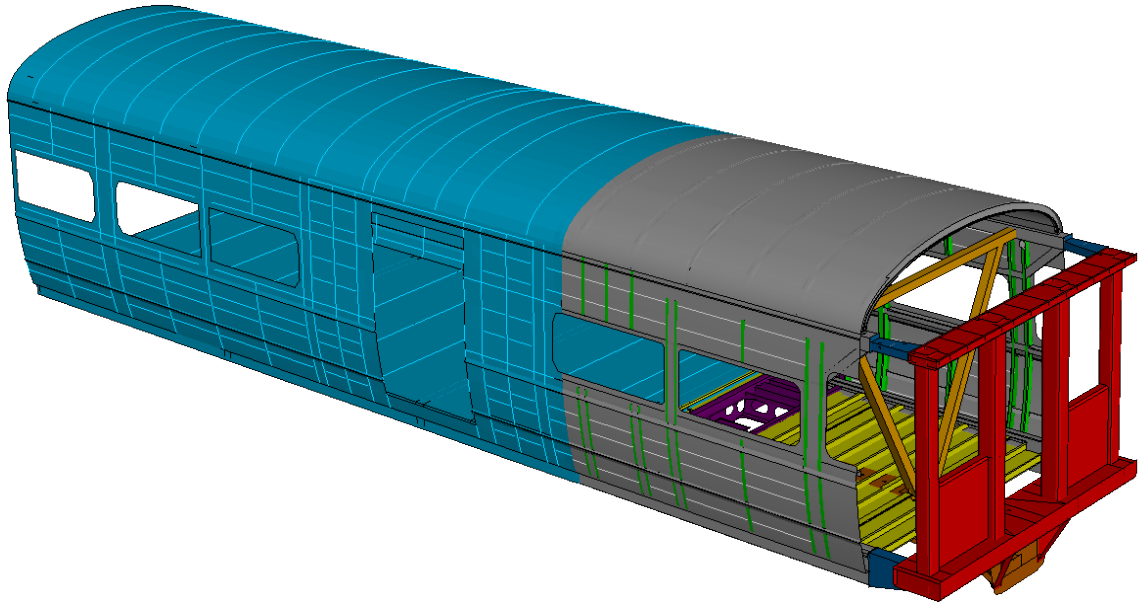
Figure 17. FE model for the full-width model of the M1 car with SOA end frame
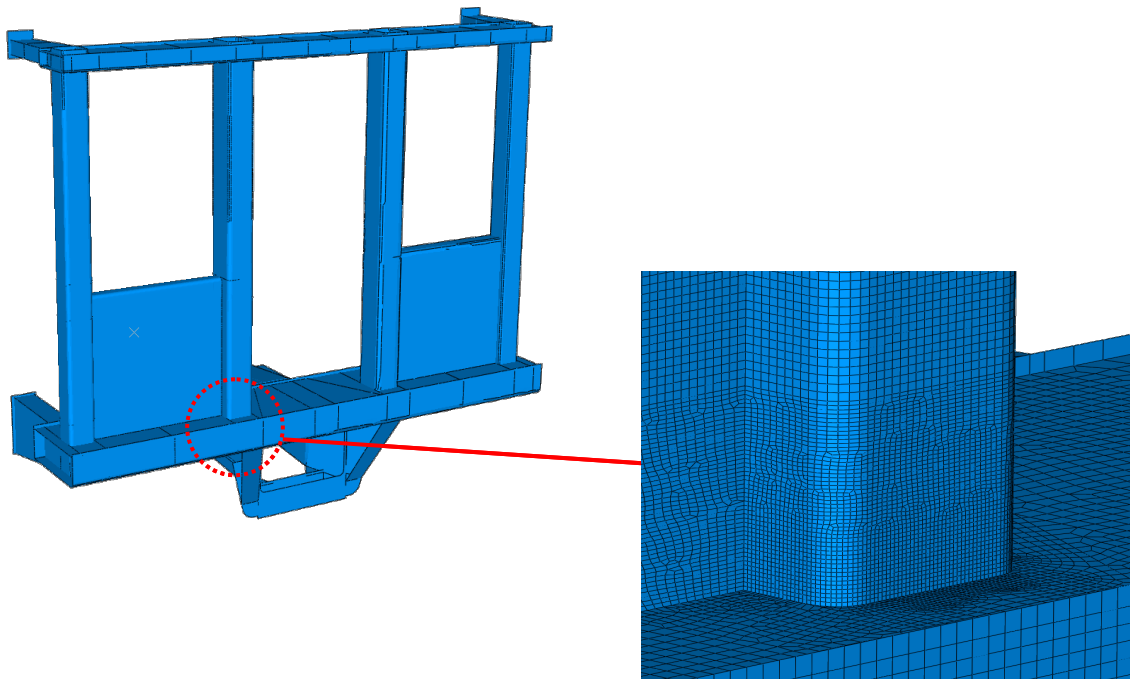
Figure 18. FE model of the end frame only, with detailed mesh around base of collision post highlighted
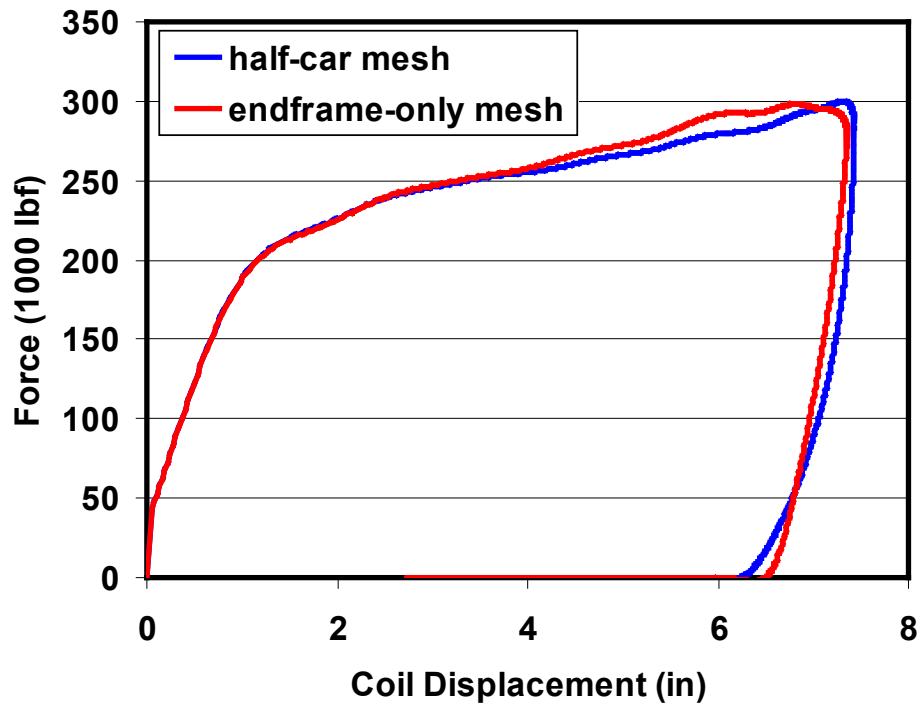
Figure 19. Comparison of force-displacement curves for dynamic collision post crush using half-car model and end-frame only model

The material models for the various steel components in the end frame were based on the material test report data listed in Table 2 for A572-50 and A656-80, and do not include failure. Several additional varieties of steel were used in the reinforced car body, including 301 series stainless. Other materials, including wood panels and corrugated sheet, were also present. The connector elements were fabricated primarily from A606-50.

5.1 Static Analyses

A series of linear and nonlinear analyses were performed to evaluate end structure behavior with respect to static load requirements. The 10 analyses conducted are listed in Table 3. Note that each analysis case corresponds to a specific requirement (section) in the APTA standard. The acceptance criterion for most of the analysis cases is the absence of permanent deformation, i.e., no stresses above yield. For these cases a linear static analysis was conducted using ABAQUS/Standard [9]. The single load case for which there is an ultimate strength requirement is the 200,000-lbf longitudinal load on the collision post, 30 inches above the underframe. For this case, a nonlinear analysis was conducted using ABAQUS/Explicit.

Table 3. Static load cases

Load (kips)	Orientation	Component	Location	Acceptance Criterion	APTA Reference*
800	Longitudinal	Car Body	Line of Draft at Buff Lug	Yield	5.1.1a)
500	Longitudinal	Car Body	End Beam Front Face	Yield	5.1.1b)
200	Longitudinal	Collision Post	30" Above U/F	Ultimate	5.3.1.3.1b)
60	Longitudinal	Collision Post	55" Above U/F†	Yield	5.3.1.3.1c)
60	Longitudinal	Collision Post	Just under AT Beam	Yield	5.3.1.3.1c)
100	Longitudinal	Corner Post	18" Above U/F	Yield	5.3.2.3.1b)
45	Longitudinal	Corner Post	55" Above U/F†	Yield	5.3.2.3.1c)
45	Longitudinal	Corner Post	Just under AT Beam	Yield	5.3.2.3.1c)
100	Lateral	Corner Post	18" Above U/F	Yield	5.3.2.3.1b)
45	Lateral	Corner Post	55" Above U/F†	Yield	5.3.2.3.1c)

* APTA SS-C&S-034-99, Rev. 2 [1]
† Midway between U/F and AT beam

Static analyses were first conducted for an initial iteration of the design. The results of these analyses revealed two minor problem areas:

- For the 500,000-lbf load applied across the front of the buffer beam, a stress concentration arose at the point where the draft gear flares out just behind the buffer beam. Although it was likely that the magnitude of this stress was partly due to the sharp corner present at this location, a triangular, horizontal stiffening plate was added (see Figure 13).

- For the 60,000-lbf longitudinal load on the collision post, FE calculations indicated that when the load was applied to the post just below its connection to the AT beam, stress exceeding yield arose in the roof connection plate due to the large moment that was created. This non-compliance was eliminated by increasing the thickness of this steel plate from 0.120 inch to 0.179 inch (see Figure 8).

With these changes, the analysis results indicated that the M1 car with the SOA end frame met all of the static load requirements.

Figure 20 shows a representative static load case result. For the 500,000-lbf load on the end of the buffer beam, high stresses arose only at the point of application of the load and at a couple of very small regions where the draft sill connected to the floor structures (and where there were sharp corners in the model). All of these high stresses were judged to be artifacts of the way the

structure was modeled and how the applied load was distributed. The stress everywhere else in the car body was lower than the yield strength of any of the materials that comprised the car structure.
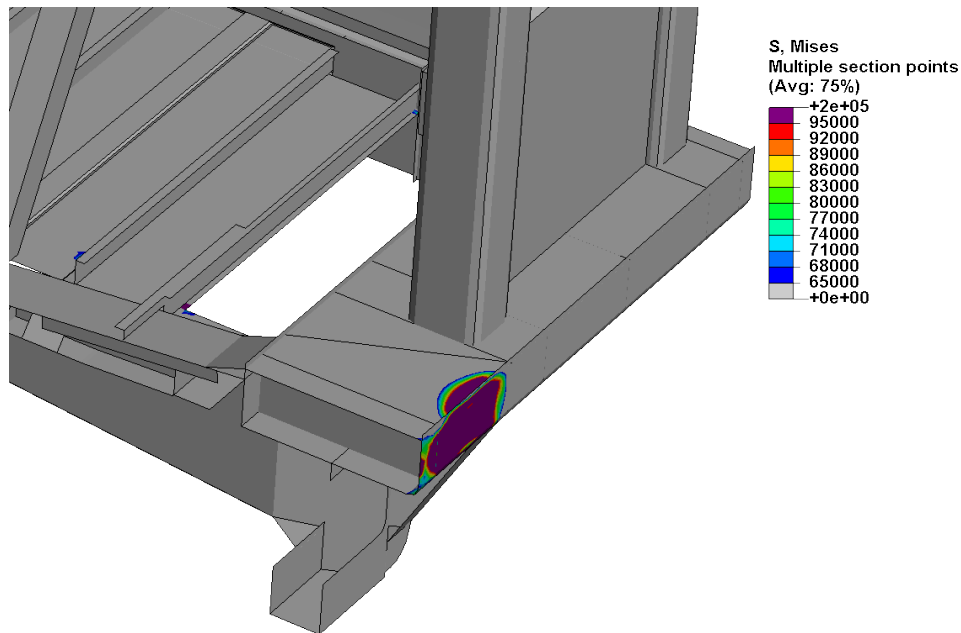
Figure 20. Predicted Mises stress distribution for 500,000-lbf load on central part of end beam

5.2   Preliminary Quasi-Static and Dynamic Impact Analyses

Prior to fabrication of the various end frame, connection and car body reinforcement components, preliminary quasi-static and dynamic impact analyses were performed to provide some assurance that the SOA end frame/M1 car retrofit design met the energy absorption requirements detailed in the FRA NPRM and the APTA standard. Note that these models did not include material failure and, as such, could not assess the effects of fracture on the ability of the end structure to meet the requirements. In recognition of this limitation, the research program described in this report was expanded so that material failure could be incorporated into the models so that this assessment could be made. The results of these models are described in Section 5.3.

5.2.1   Quasi-Static Analyses

Preliminary quasi-static analyses were performed using ABAQUS/Explicit. The mesh for the collision post load case is shown in Figure 21. For this analysis, the load was applied via a rigid block that was 10 inches high and as wide as the post. (The geometry of the load application block was later changed to that of the coil-shaped structure ultimately used in both the dynamic and quasi-static tests.) For the corner post load case, the load plate was re-positioned to the corresponding location on that post. The rigid load application block was gradually displaced a total distance of 10 inches.
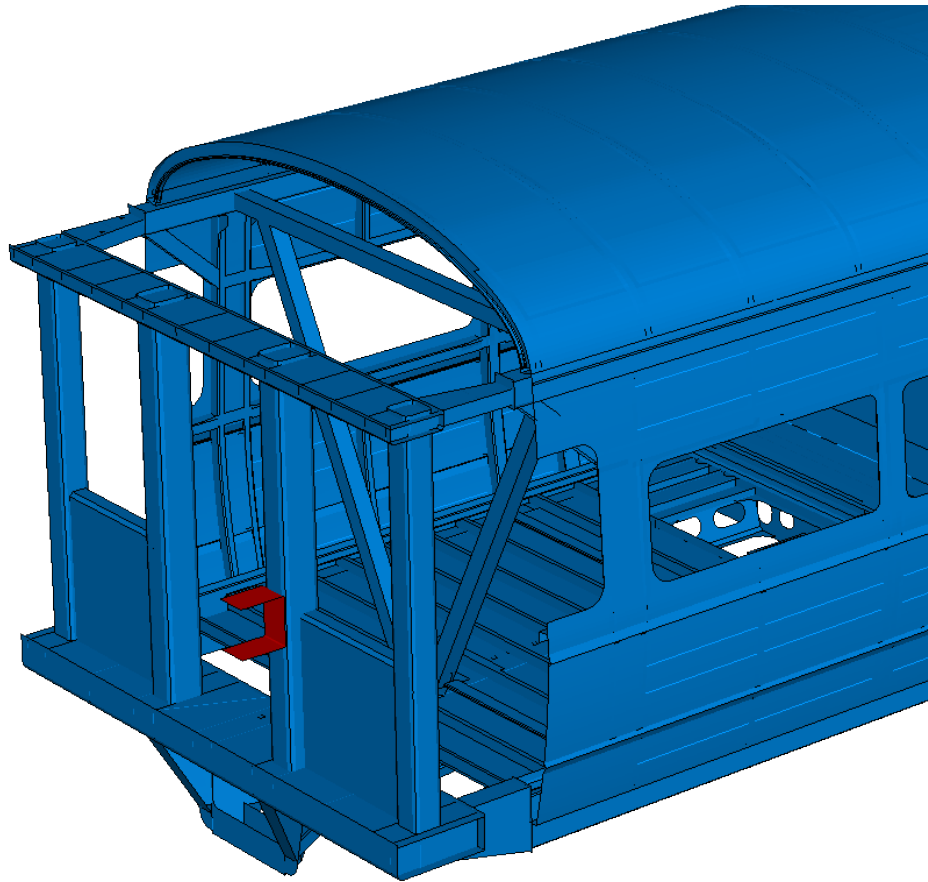
Figure 21. Forward end of the finite element model of the quasi-static collision post load case, with the load application block highlighted

The deformation of the end frame that arose when the collision post was displaced by 10 inches is shown in Figure 22. Plastic deformation was generally confined to the loaded collision post, the attached shelf/bulkhead plate, the AT beam above the loaded post, and the corner post – just where it connected to the shelf. There was a also a slight deformation of the side sill and roof rail connection plates on the loaded side of the car, but essentially no deformation in the reinforced car body, behind the connections to the end frame, as was desired. Contours of equivalent plastic strain shown in Figure 22 indicate that high levels of plastic strain arose at the front base of the collision post and at the back of the post opposite the point of load application. At the base of the post, the equivalent plastic strain reached about 37 percent. At the back of the post, opposite the load application point, the equivalent plastic strain reached 22 percent.
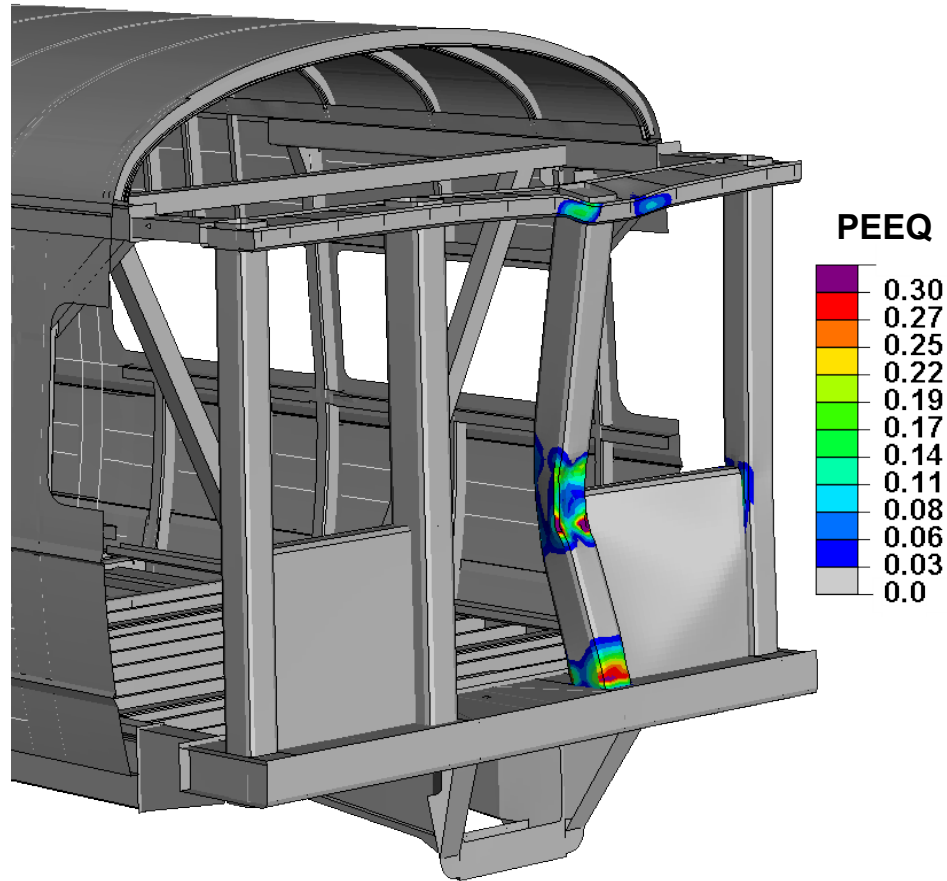
Figure 22. Contours of equivalent plastic strain for the quasi-static collision post load case

Similar results were predicted for the corner post quasi-static load case. The predicted deformation at 10 inches of load point displacement is shown in Figure 23. For this case, the deformation was localized to the corner post, the shelf where it connected to both the collision and corner posts, the bulkhead plate, the AT beam where it connected to the corner post, and both the side sill and roof rail connection members. The equivalent plastic strain reached 19 percent at the front base of the corner post and 28 percent at the back of the post opposite the load point.
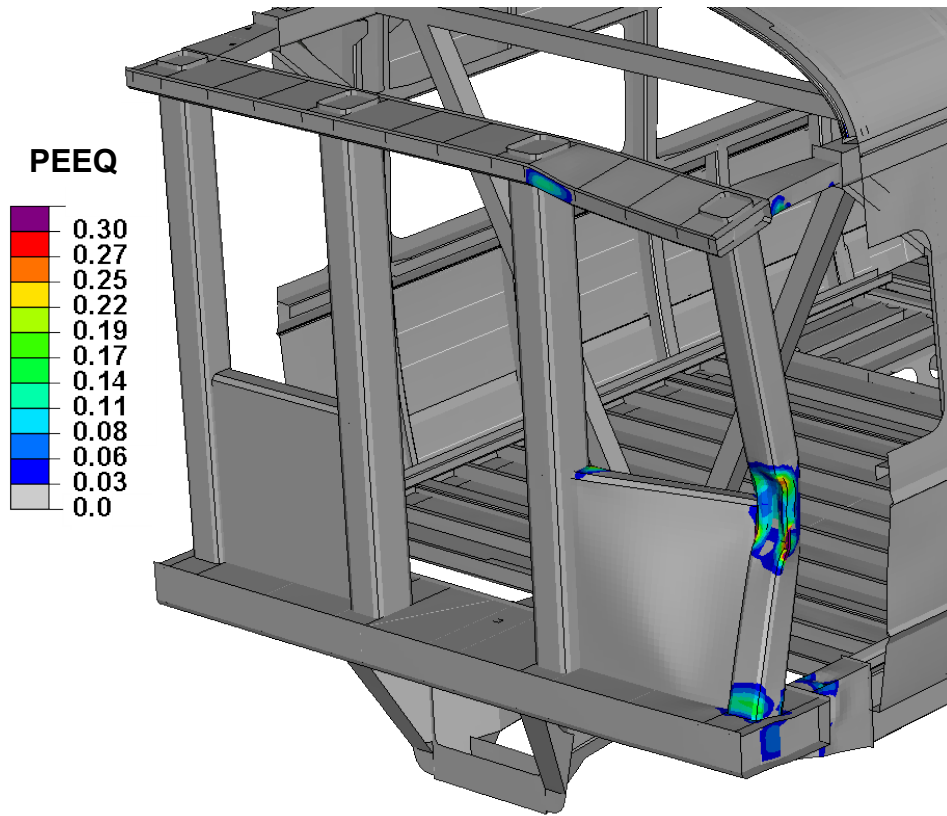
Figure 23. Contours of equivalent plastic strain for the quasi-static corner post load case

5.2.2 Dynamic Impact Analyses

A similar set of analyses were run to simulate dynamic impact test conditions. The mesh for the collision post impact case is shown in Figure 24. For the dynamic analyses, the coil was assigned a mass of 10,000 lbm and an initial velocity equal to 21 mph for the collision post impact and 20 mph for the corner post impact.
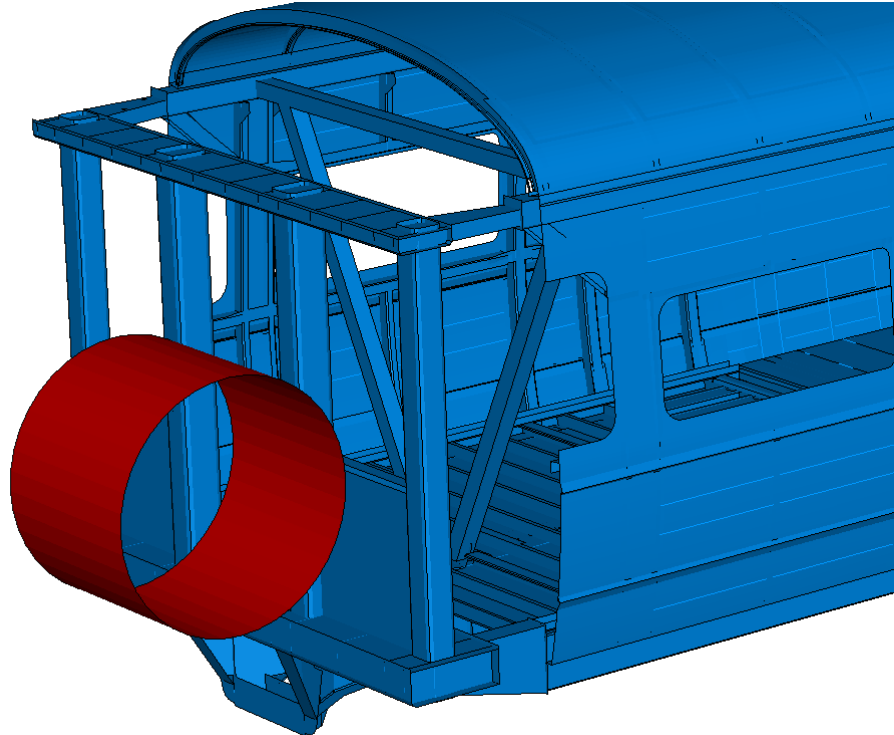
Figure 24. FE model of the dynamic coil impact of the collision post load case

The deformation modes for these analyses were very similar to those depicted in Figure 22 and Figure 23 for the quasi-static cases. For the collision post case, the coil deflected by 7.4 inches into the post before rebounding off. The back of the collision post intruded into the occupied volume by 6.4 inches. (The difference between these two values was due to local crushing of the post.) Equivalent plastic strains of 29 percent and 16 percent arose at the front base of the post and the back of the post opposite the point of impact, respectively. These values were smaller than those predicted by the quasi-static load case at a deformation of 10 inches, but were quite consistent with quasi-static predictions at corresponding levels of displacement.

For the corner post impact case, the coil deflected by 8.3 inches, and the post intruded into the occupant volume by 8.0 inches. The larger displacement relative to the collision post case was due to the much smaller post size, which more than offset the use of a stronger material (A656-80) than that used in the collision post (A572-50).

5.2.3 Predicted Energy Absorption

A comparison of the load-displacement curves for all four quasi-static and dynamic load cases is shown in Figure 25. Note that the plotted displacement is that of the coil or load application block. The displacement at the back of the post was generally a little smaller due to deformation of the post at the load point. As expected, the corresponding curves are similar. The calculated energy absorption is plotted in Figure 26. Note that energy was calculated here as the area under the force-displacement curve. For the quasi-static collision post load case, when the deformation energy reached the required level of 135,000 ft-lbs, the displacement was 6.5 inches – versus 6.9 inches for the dynamic case. For the quasi-static corner post load case, when the deformation energy reached the required level of 120,000 ft-lbs, the displacement ass 8.0 inches – versus 7.7 inches for the dynamic case.
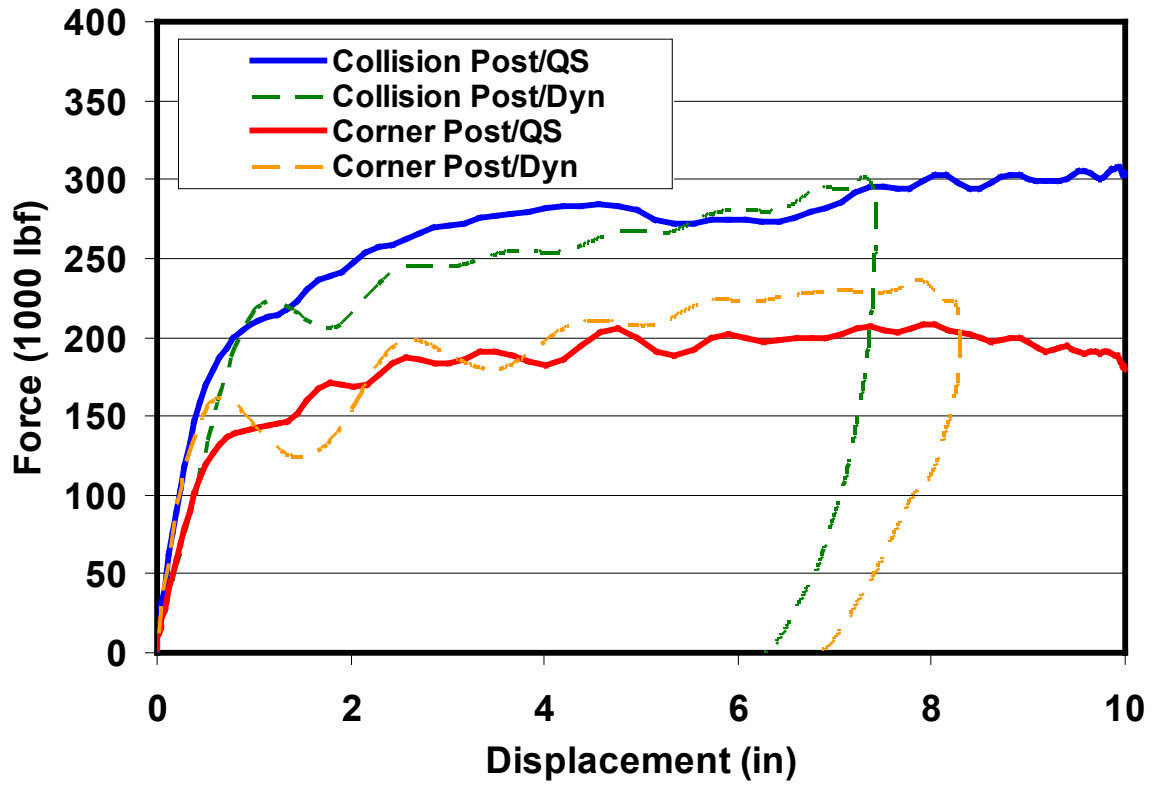
Figure 25. Comparison of force-displacement results for the four quasi-static and dynamic impact cases
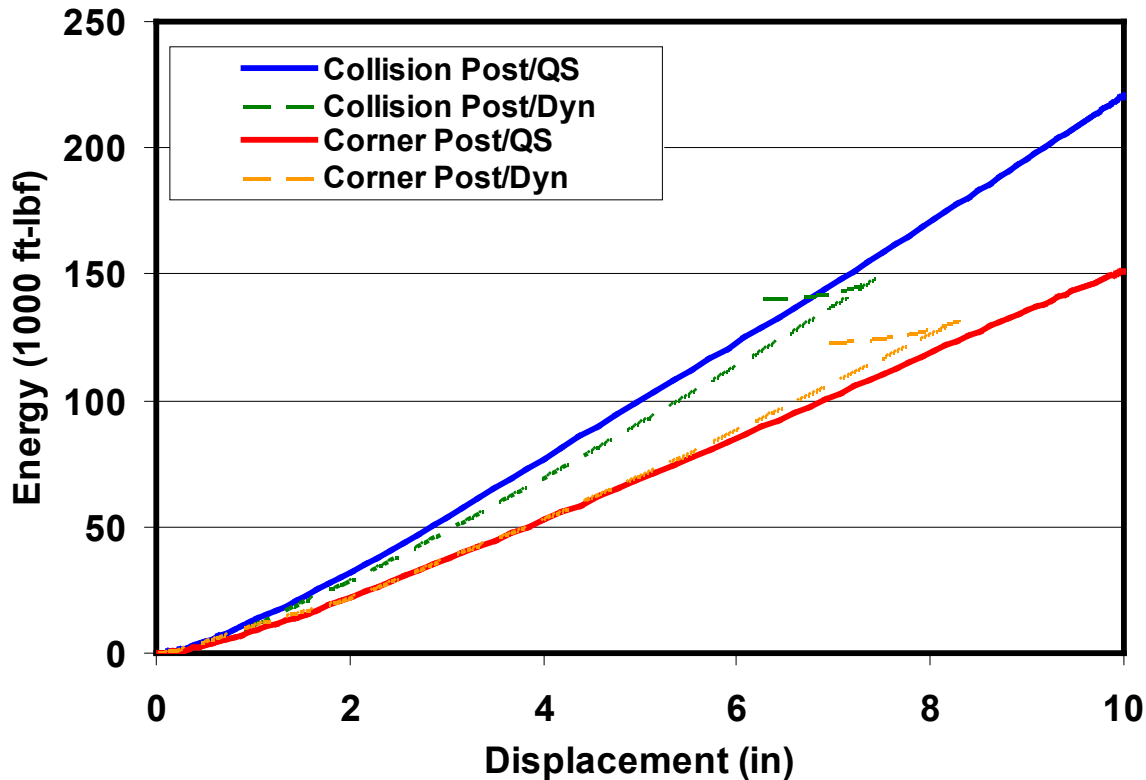
Figure 26. Comparison of energy-displacement results for the four quasi-static and dynamic impact cases

Based on these results, the design was determined to be in compliance with the energy absorption requirements of the FRA NPRM and the APTA standard, and fabrication of the end frame components commenced. However, since these analyses did not include failure, they could not assess whether material failure would occur to the extent that the post would separate from its attachments or fail to achieve the energy absorption requirements. A new set of calculations that included material failure were performed to make this assessment. These calculations were performed in parallel with the tests and are described in Section 5.3.

5.3 Simulation of Quasi-Static and Dynamic Impact Tests

Based on the results of the dynamic corner post impact test (conducted in 2002), some fracture was expected in certain key end frame components during the three tests conducted in 2008. For this reason, a material failure model based on the Bao-Wierzbicki fracture criterion [3] was implemented in the FE model of the cab car end frame using ABAQUS/Explicit. The FE model with material failure was used to assess the effect of fracture on the deformation behavior of cab car end structures during quasi-static loading and dynamic impact and, in particular, on the ability of these structures to absorb energy.

The failure model was implemented in ABAQUS/Explicit for use with shell elements. A series of preliminary calculations were first conducted to assess the effects of element type and mesh refinement on the deformation and fracture behavior of structures similar to those found on cab car end frames, and to demonstrate that the Bao-Wierzbicki failure model could be effectively applied using shell elements. Model parameters were then validated through comparison to the

35

results of the 2002 test. A description of the material failure model, results of preliminary calculations, and results of the model validation analysis are detailed in [10] and summarized in Appendix D.

With material failure incorporated into the FE model and with the material parameters fit to the results of the 2002 test, analyses were conducted to predict the results of the three tests performed in 2008 (dynamic impact of a collision post, quasi-static loading of a collision post, quasi-static loading of a corner post). After each test, model predictions were compared with test results. Based on these comparisons, modifications were made to the model as required.

Schematic illustrations of the configurations for the single dynamic and two quasi-static tests are shown in Figure 27 and Figure 28.
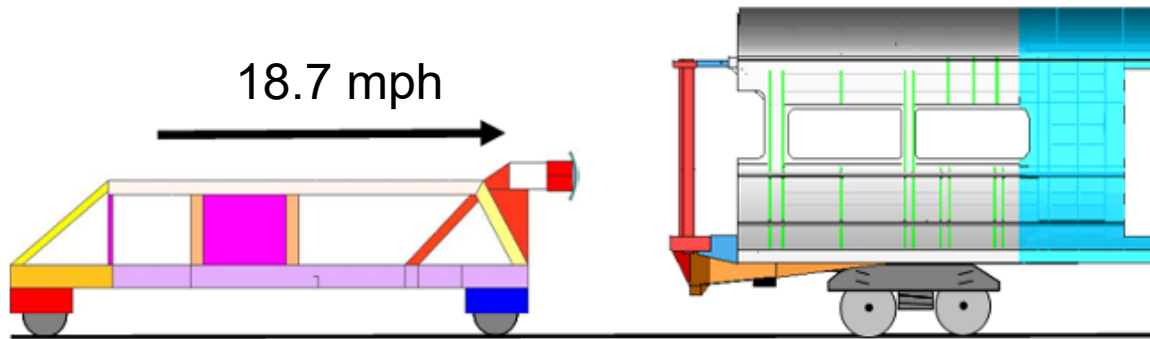
Figure 27. Schematic illustration of the dynamic impact test
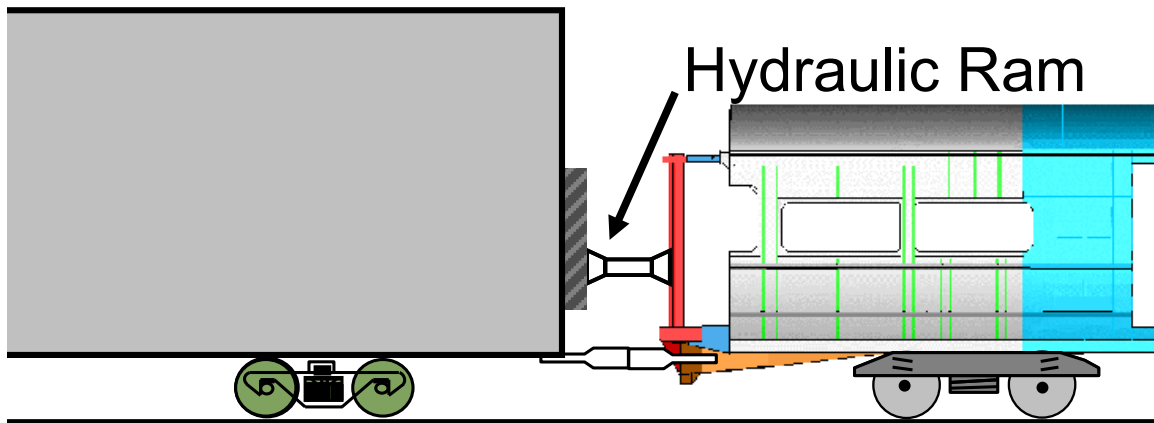
Figure 28. Schematic illustration of the quasi-static test

For the dynamic test (Figure 27), a cart, mounted with a coil-shaped steel impactor at its leading end, was developed as an alternative to the arrangement used in the 2002 test [6]. The impactor had a diameter of 48 inches and a width of 36 inches. It was positioned at the required height of 30 inches above the floor of the cab car and centered on the collision post located on the right hand side of the cab car. The finished cart weighed approximately 14,000 lbm, and the cab car weighed about 70,000 lbm. The measured impact speed was 18.7 mph. A description of these tests can be found in [6, 7].

For the quasi-static tests (Figure 28), the test car was coupled to a reaction car. Load was applied to a single collision or corner post through a hydraulic ram suspended from a crane. The load was reacted through the couplers of the two vehicles, with the draft gears of each car replaced with rigid steel blocks. The applied force was measured using a set of four load cells positioned in series with the ram. Displacement was measured at a number of locations using string potentiometers.

5.3.1 Dynamic Collision Post Impact Test

The dynamic collision post impact test was conducted in April 2008. Pre-test model predictions of this test indicated that fracture would occur at the front base of the collision post, at its connection to the end frame, much like what occurred in the corner post test. The deformed post is shown in Figure 29. Deformation of the post into the occupied volume was predicted to be 6.4 inches.
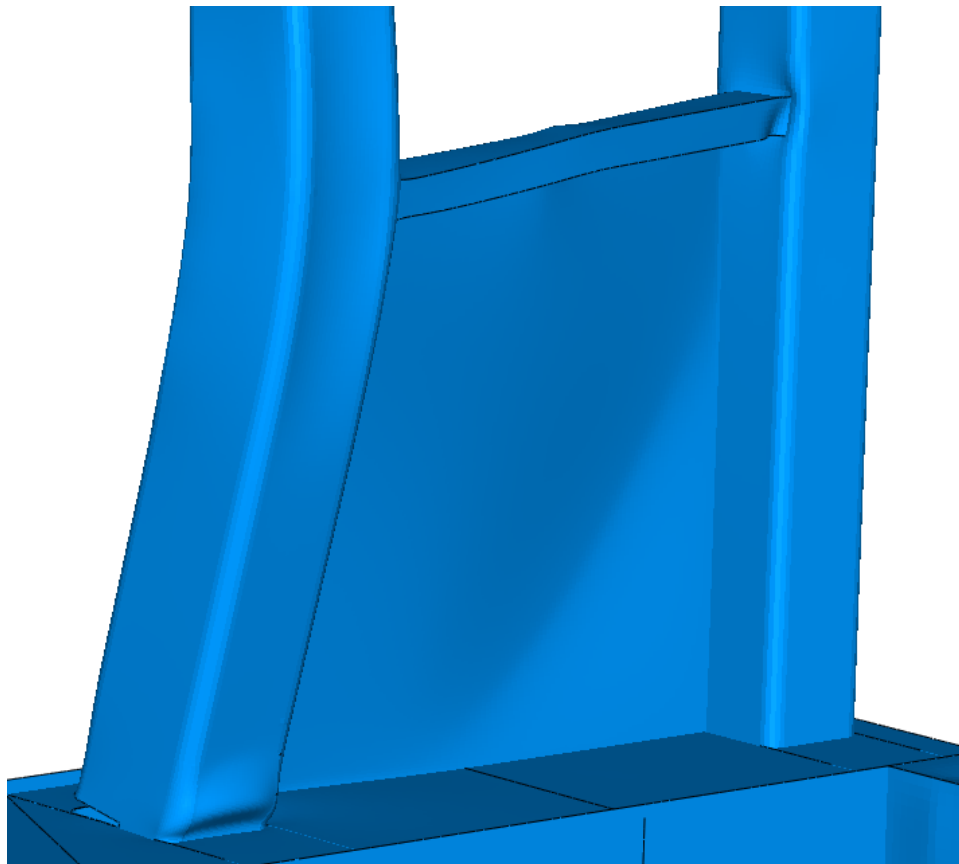
Figure 29. Pre-test prediction of collision post deformation following the dynamic collision post impact

A photograph taken following the test, shown in Figure 30, indicates that not only was the fracture at the front base of the post slightly more extensive than predicted, but that fracture also occurred at the rear of the post, behind the point of impact.
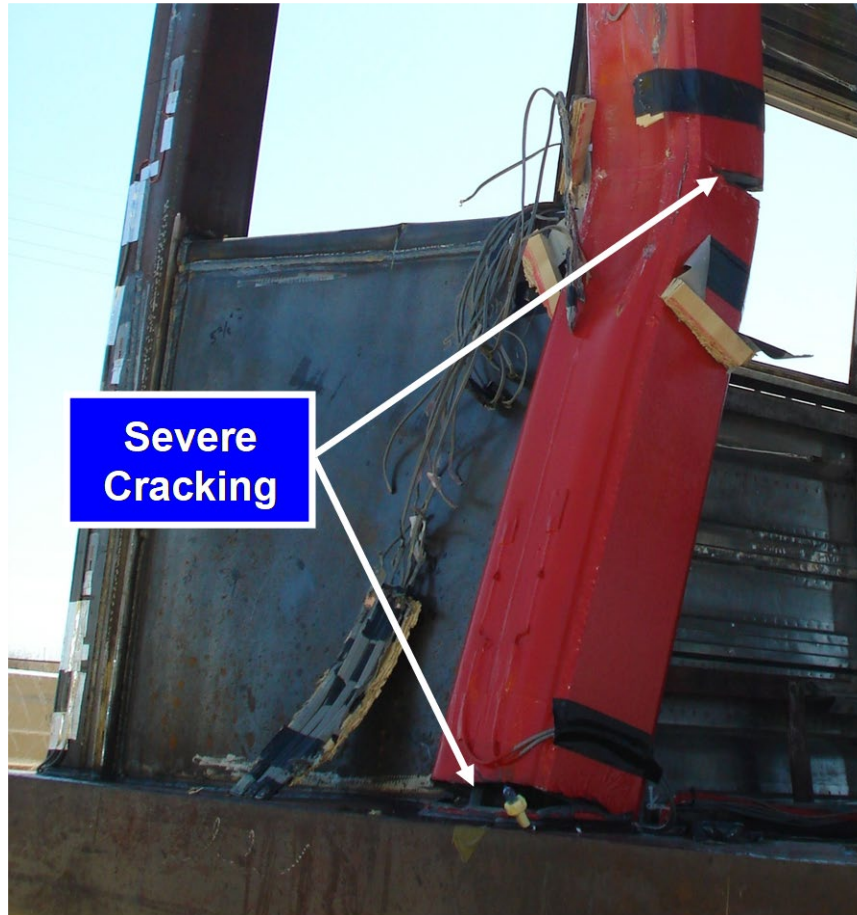
Figure 30. Dynamic impact test – fracture occurred at the front base of the post and at the back of the post, opposite the point of impact

An inspection of the fracture at the back of the post following the test revealed that it occurred at a location where both an internal gusset and an external tab are welded to the post (see Figure 31). The fracture, in fact, occurred along the edge of one of the two welds. These details, which were not in the original model, were subsequently added and the analysis was run again. Material failure model parameters were adjusted so that the extent of fracture was more consistent with the test results.

Note that the material used to fabricate the collision posts was A572-50. This material exhibits ductility limits that are similar to, but not the same as, the A710 steel used in the corner post for the 2002 test. Strength data used in the material model were based on certifications provided with the A572-50 plates from which the collision posts were fabricated. It was necessary to extrapolate these data to form a complete stress-strain curve for this material. Based on the results of some supplemental calculations, it appeared likely that much of the difference between the values of the failure parameters found to be optimal for modeling A572-50 behavior in this test and those that were found to be optimal for modeling A710 behavior during the 2002 corner post impact test was attributable to differences in the hardening behavior assumed for the respective material models.
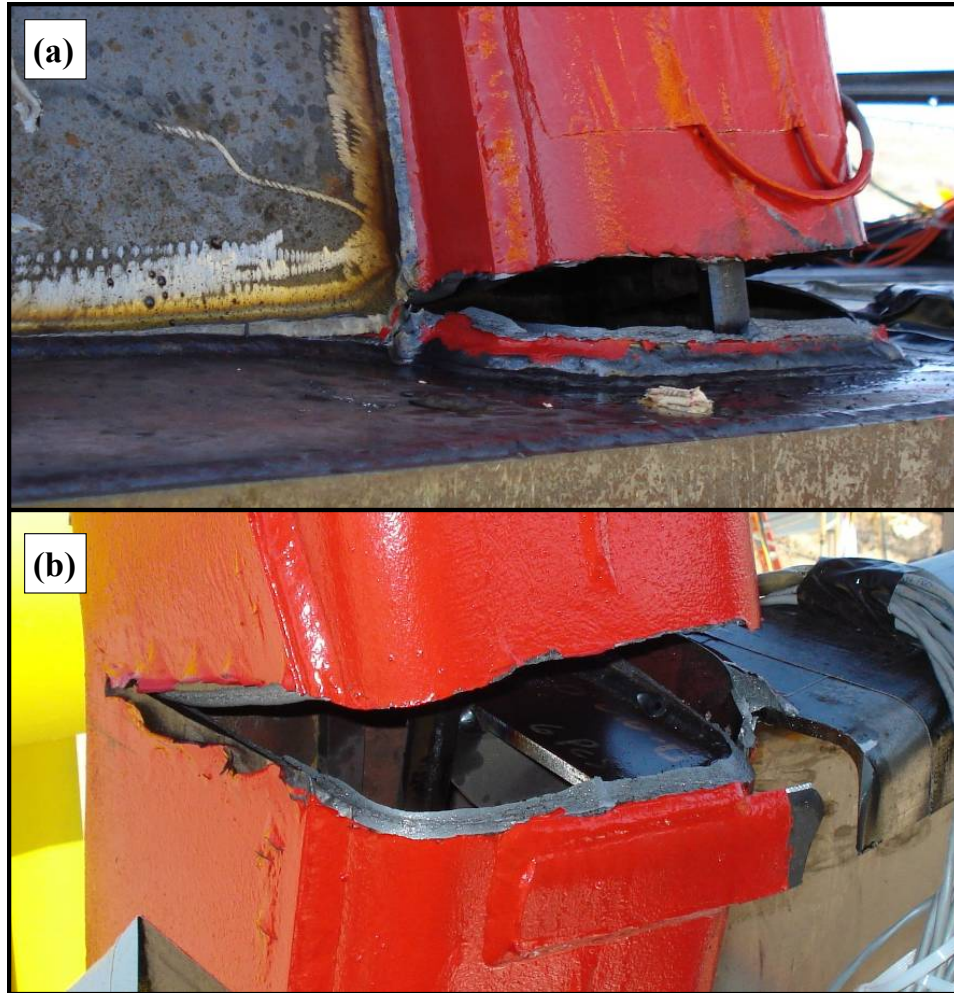
Figure 31. Post-test photographs showing fracture regions: (a) front base of the collision post and (b) in back of the collision post, opposite impact point

With these changes to the failure parameters used in the FE model of the collision post impact, the calculated extent of fracture and deformation of the post was consistent with test results, as illustrated in Figure 32. The predicted extent of collision post permanent deformation was found to be 6.9 inches. This was an increase from 6.4 inches for the baseline model and compared favorably to the measured deformation of 7.4 inches.
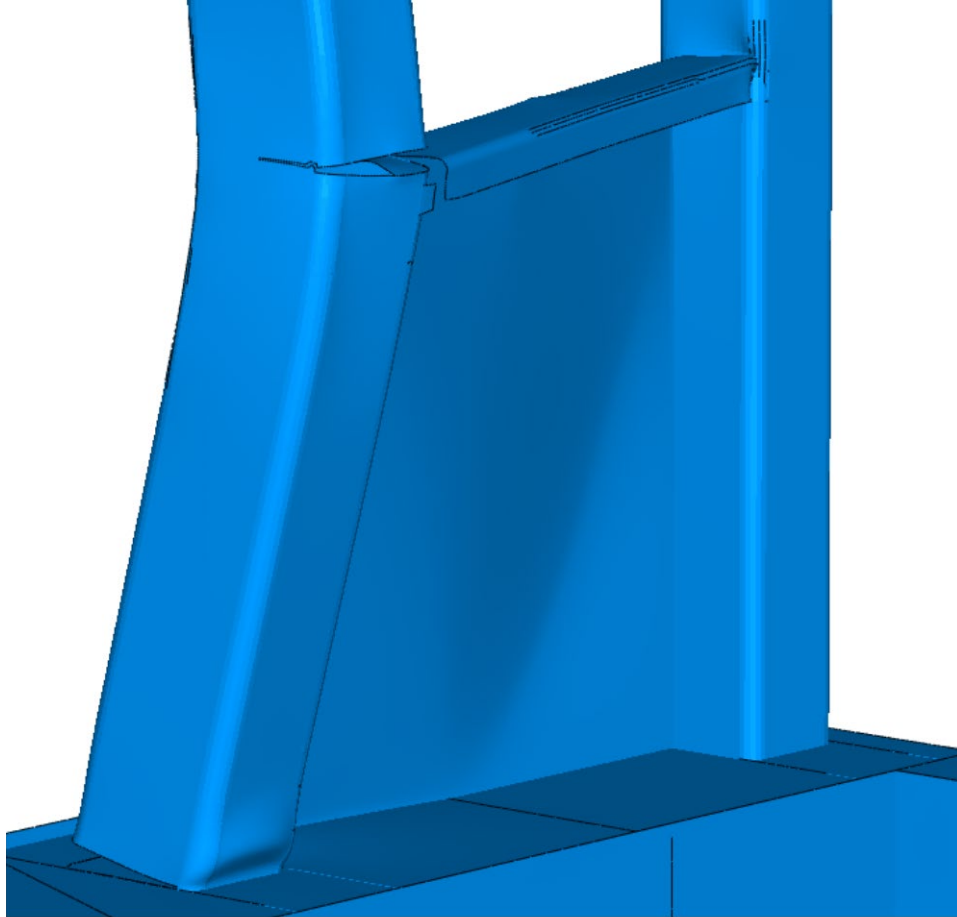
Figure 32. Predicted deformation of the collision post following the dynamic collision post impact (revised model)

5.3.2 Quasi-Static Collision Post Crush Test

The FE model was next used to predict the results of the quasi-static collision post test. As shown in Figure 33, the model predicted that the load would rise to about 260,000 lbf after 3 inches of post displacement, whereupon fracture would initiate at the front base of the post. Fracture at the back of the post was not expected to occur until after about 8 inches of post displacement. The required 135,000 ft-lbf of energy absorption was predicted to be reached after only 7.7 inches of crush. Figure 34 shows the predicted deformation of the end frame after loading ram displacement of 8 inches (failure initiation behind post) and 14 inches (complete failure of post).
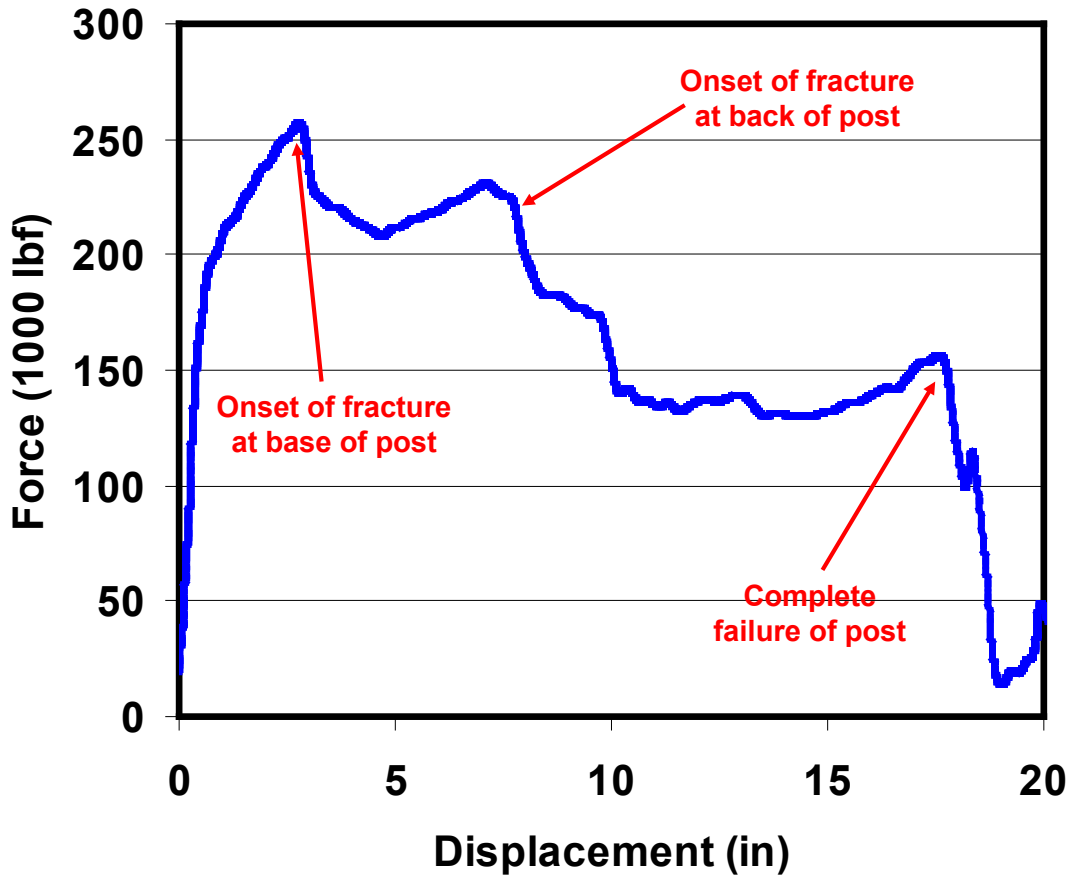
Figure 33. Predicted deformation of the collision post during the quasi-static load test
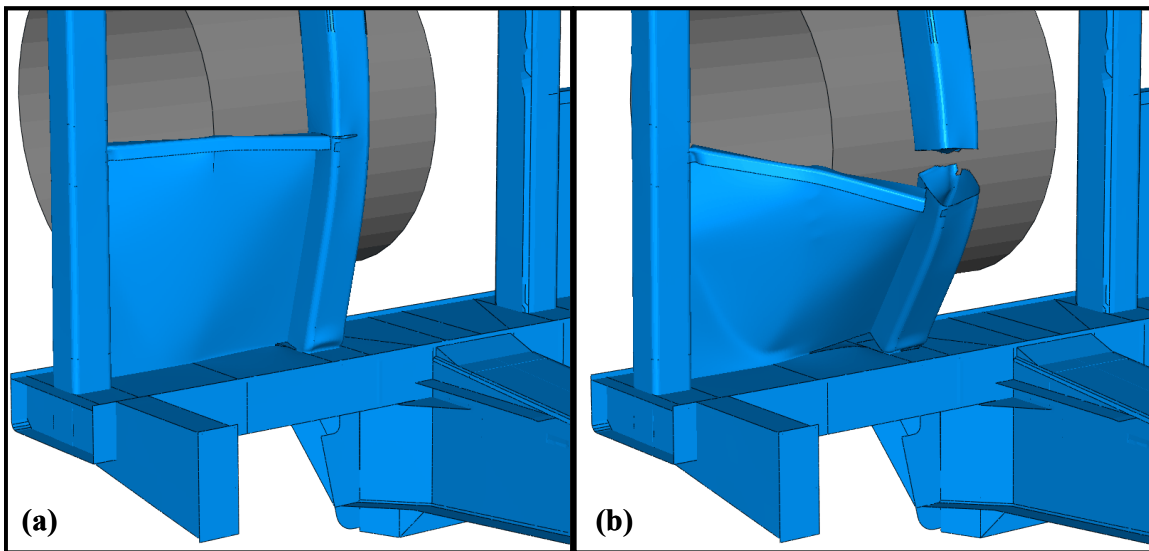
Figure 34. Predicted deformation of the SOA end frame after: (a) 8 inches of ram displacement (failure initiation behind the post and (b) 14 inches of ram displacement (complete separation of post)

41

In the subsequent test, as shown in Figure 35, fracture occurred first at the back of the post at a load of about 215,000 lbf after only about 2 inches of displacement. Fracture at the front base of the post initiated after approximately 2 additional inches of displacement. Overall, the deformation behavior observed during the test was considerably different than the model prediction.
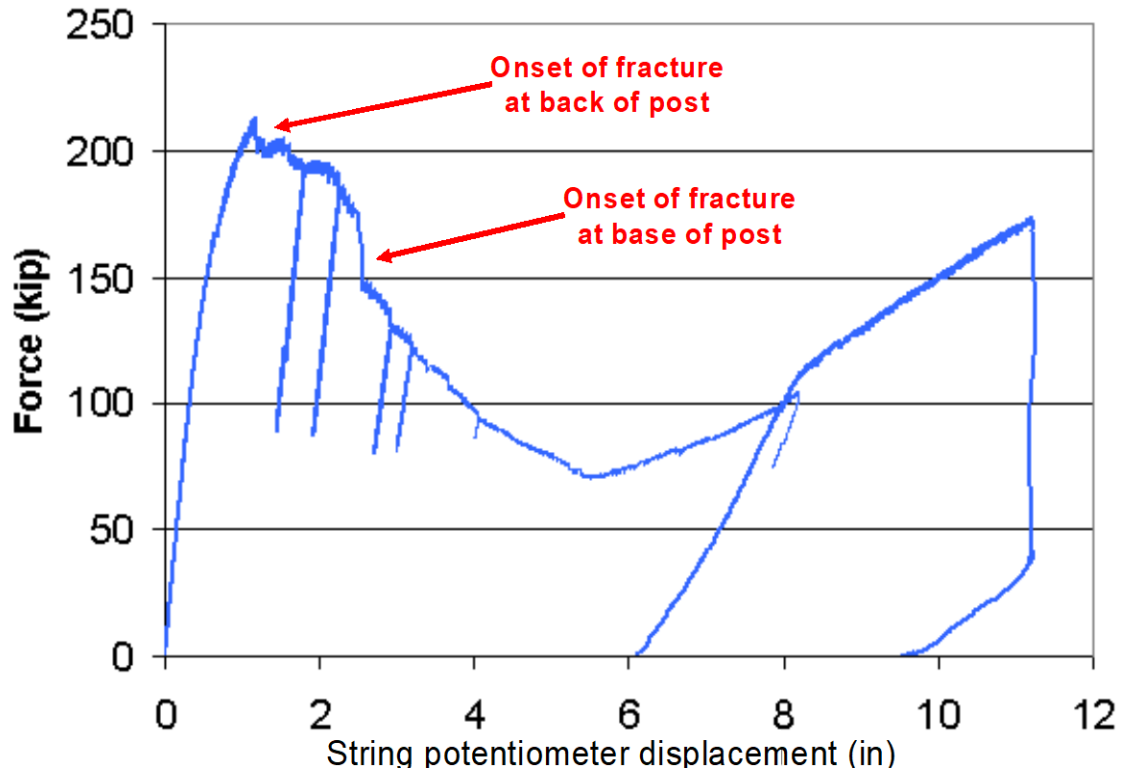
Figure 35. Measured deformation of the collision post following the quasi-static collision post impact

As a result of the poor behavior observed in this test, an investigation of the causes of premature fracture at the back of the post was initiated. Specimens were cut out of the collision post, both in the region of the unexpected fracture and away from this region. Similar specimens were cut out of the corner post. Some of these specimens were tested in three-point bending [11]. A post-test photograph of a specimen cut across a pair of collision post-to-shelf tab welds is shown in Figure 36. As is evident, the specimen had undergone substantial bending without showing any signs of incipient failure. The peak strain in the outer fiber of the bend was estimated to be nearly 20 percent. In general, the results of these tests indicated that the ductility of the materials in this region were not significant factors contributing to the premature fracture.

Figure 36. Post-test photograph of a specimen cut out from the collision post, across the shelf tab weld

Photographs of sections taken across the fracture that occurred behind the collision post in both the dynamic and quasi-static tests are shown in Figure 37. As is evident in this figure, in both cases the fracture occurred where there was a weld on the inside of the post (for an internal gusset) and on the outside of the post (for a strap that tied the shelf to the back of the post).
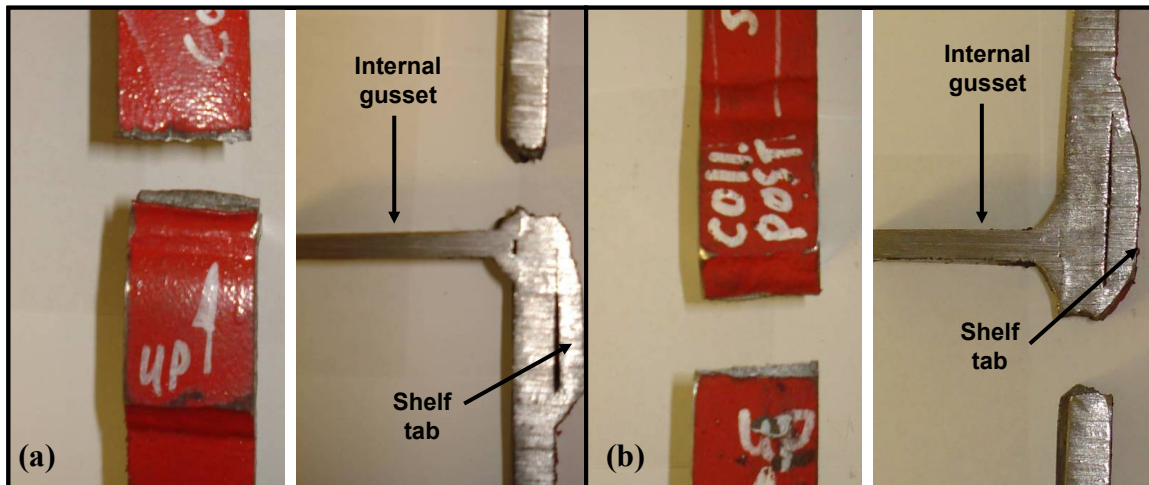
Figure 37. Photographs showing cross-sections of fractures that occurred at the back of the collision post during (a) the dynamic test and (b) the quasi-static test

It was concluded, based on these cross-sections and the results of the bending tests, that the rigidity imparted to the post by the internal gusset and the strap that tied the back of the shelf into the back of the collision post placed severe limitations on the ability of the post to deform in this region, with the net result that it behaved in a relatively brittle manner, despite the fact that the A572-50 material from which the post was constructed is quite ductile.

43

Based on this evaluation, the shelf connecting the collision post to the corner post was modified so that it was not as deep and would connect only to the side of the posts, as shown in Figure 38. The shelf tab and the internal gusset were both removed. Note that the corner post was not designed to have an internal gusset.

Before Modification   **After Modification**
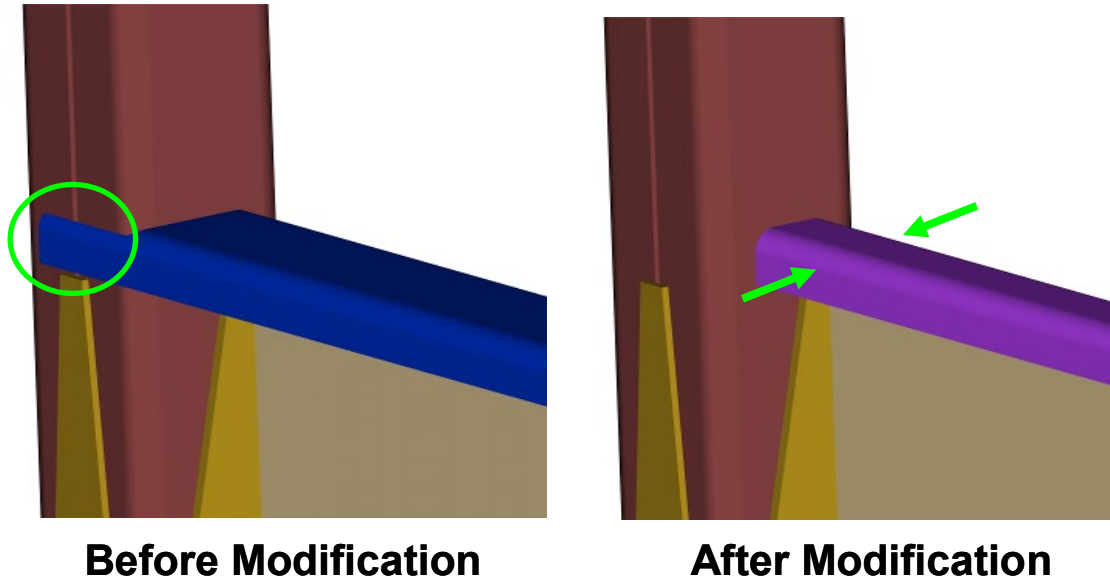
Figure 38. Schematic illustration of modifications to shelf connecting collision and corner posts

5.3.3 Quasi-Static Corner Post Crush Test

The model was revised to reflect the changes made to the design of the shelf and the removal of the internal gusset, and was then used to make pre-test predictions of the results of the quasi-static corner post crush test. Model predictions are compared with test results in Figure 39 through Figure 43. The predicted deformation of the end frame after about 10 inches of crush is compared with a photograph taken during the test in Figure 39. As is evident, predictions of the deformed shape of the end frame compared favorably with the test results in several respects, including:

- Deformed shape of the corner post

- Bending down of the AT beam

- Extent of fracture at the front base of the corner post

- Plastic deformation in both the roof and side sill connector elements

- Presence of a small fracture where the shelf meets the corner post.

- Vertical fracture at the connection of the shelf and bulkhead to the collision post

- Absence of fracture and the deformed shape of the back of the post, opposite the load point
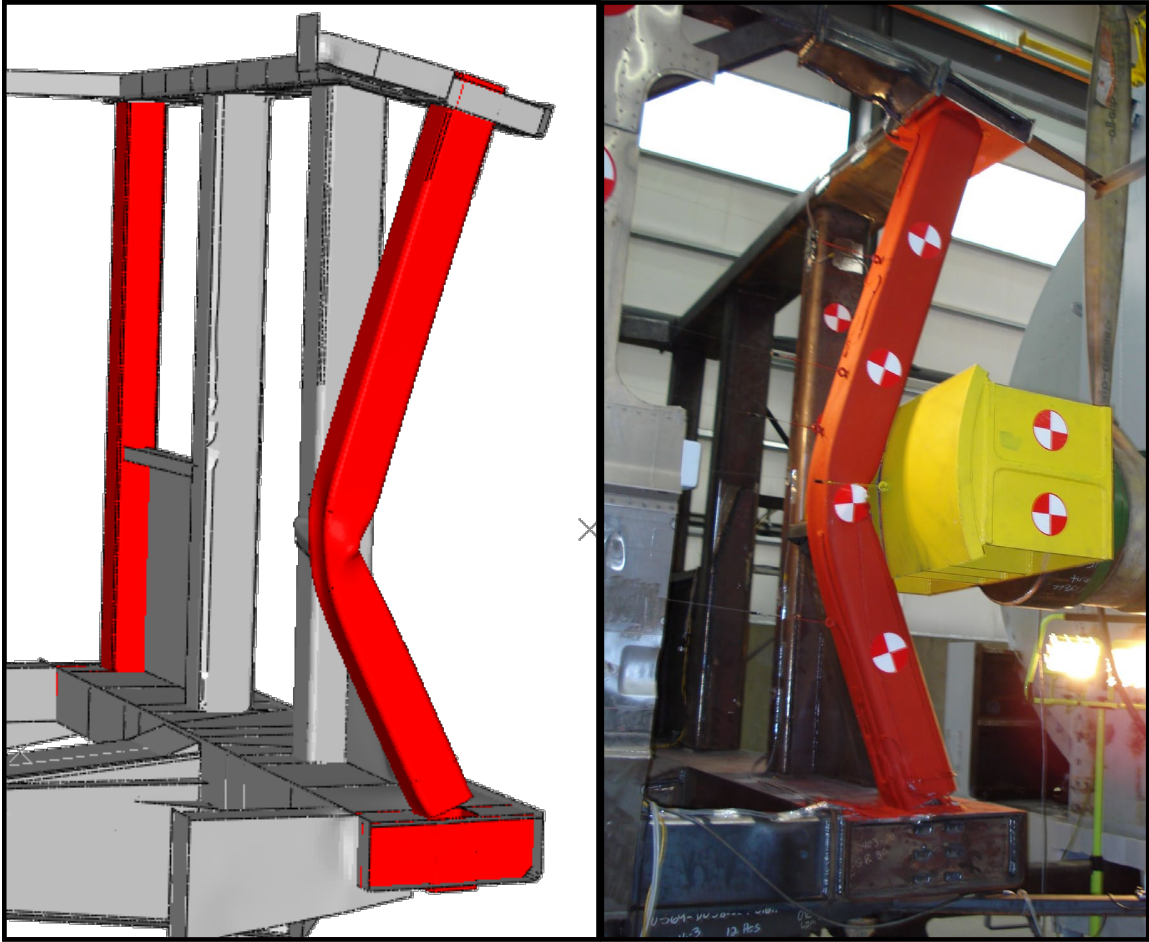
Figure 39. Comparison of predicted (left) and measured end frame deformation during corner post quasi-static crush test

Detailed views of the back of the collision post, opposite the loading point (see Figure 40) further illustrate the excellent agreement between model predictions and test results. The model clearly captured the "puckering in" of the rear wall of the corner post as well as the outward folding of the side walls just above the shelf connection and the initiation of fracture at the connection of the shelf to the corner post. The large extent of deformation without failure that the post exhibited at this location was in clear contrast to the brittle fracture mode observed at this location in both the dynamic and quasi-static collision post tests (see Figure 31). The ability of the post – which did not have an internal gusset – to deform at this location clearly seems to have been a fundamental difference between the behaviors observed in the two types of tests (i.e., collision post load tests versus corner post load test).

Fracture has initiated here

Figure 40. Comparison of predicted (left) and measured end frame deformation during corner post quasi-static crush test – detail showing back of corner post, opposite load application point

A view of the connection of the shelf and bulkhead to the collision post (Figure 41) shows that the model also captured the tearing away of the shelf/bulkhead from the post The tear started at the shelf and worked its way down the bulkhead as the post deformed.
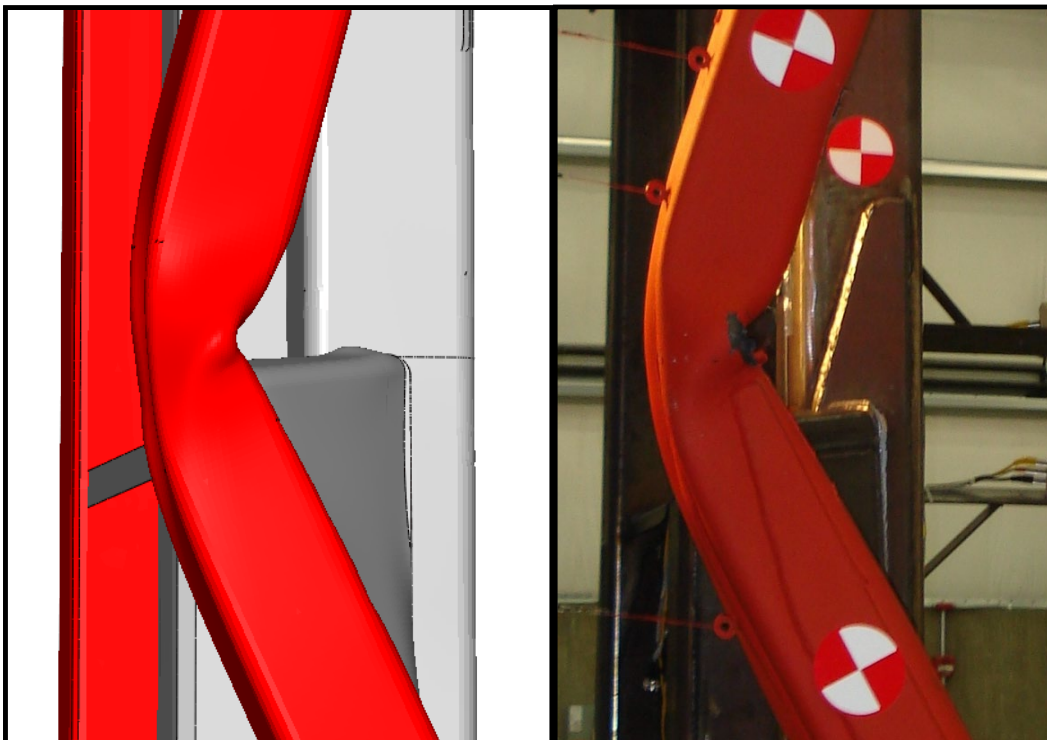
Figure 41. Comparison of predicted (left) and measured end frame deformation during corner post quasi-static crush test – detail showing back of connection of shelf/bulkhead to collision post

Predictions of force-displacement behavior are compared to test results in Figure 42. Also plotted in this figure is the prediction of force-displacement behavior using a model that did not include material failure. Failure at the front base of the post was predicted to occur after 5 inches of crush. Test results indicated that the failure occurred at this location after about 4.5 inches of crush. Following the initiation of the failure, the load continued to decrease for several inches of displacement before beginning to rise again. The actual drop in load was more significant than the model predicted. This was likely due to differences between the assumed post-initiation response of the material and the actual behavior. Despite this difference, the overall agreement between the predicted curve and the measured curve was excellent. The difference between these two curves and the curve that corresponds to the model prediction without failure clearly illustrated the advantages of accounting for material failure.
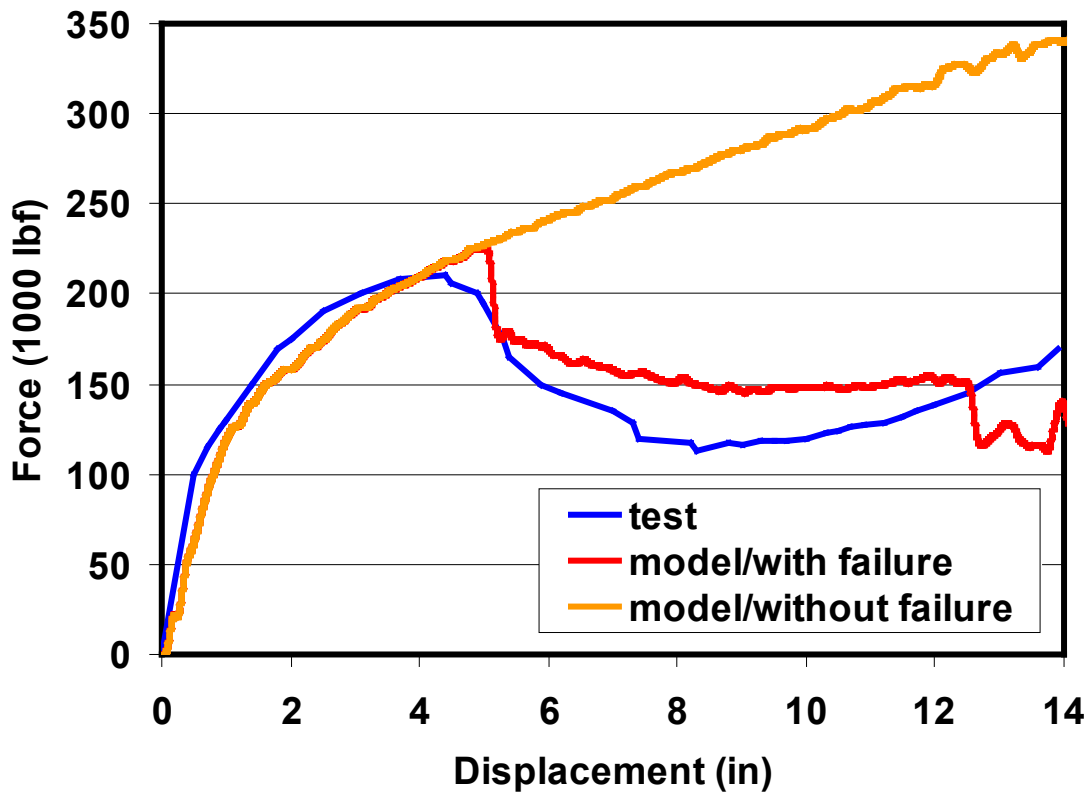
Figure 42. Measured deformation of the collision post following the dynamic collision post impact

Predictions of energy-displacement behavior are compared to test results in Figure 43. The measured energy absorption after 10 inches of post crush (125,000 ft-lbf) was just a few percent less than the value (133,000 ft-lbf) predicted by the model. This difference was probably attributable to the greater drop in force following the initiation of failure observed in the test. Once again, the difference between these two curves and that for the model without failure highlighted the advantages of material failure modeling.
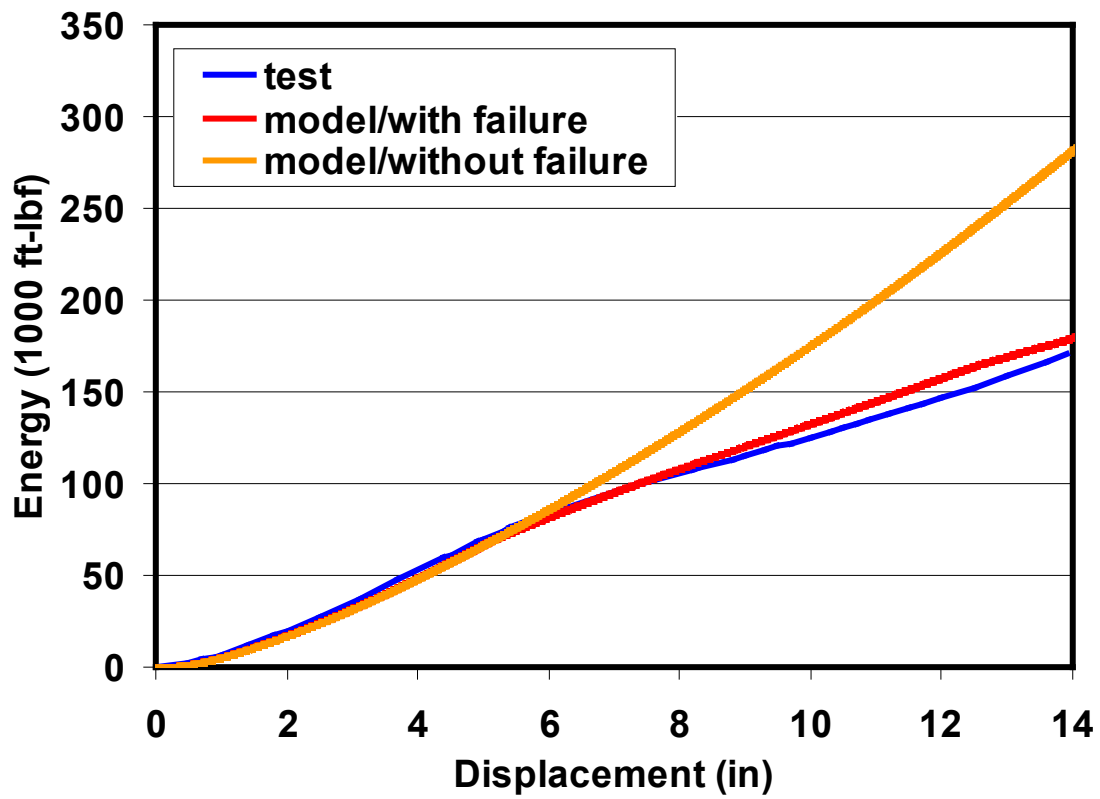
Figure 43. Energy absorption of the collision post following the dynamic collision post impact

6. Conclusion

The primary objective of the research program described here was to design and oversee the construction of a retrofit of the SOA end frame onto an M1 car so that it could be used for quasi-static and dynamic testing. While there were some challenges to overcome, particularly in regards to the premature fracture of the collision post opposite the load point that occurred in both the dynamic and quasi-static collision post tests, it is fair to say that this objective was clearly achieved. The three end frames were fabricated, assembled, and tested as planned, and the M1 car body was not damaged during any of the tests, enabling its re-use for subsequent tests.

The secondary objective of this research was to help assess whether the two test methods specified in the FRA NPRM and the APTA standard offer equivalent means of verifying the energy absorption characteristics of the cab car end structure. The modes of deformation and fracture observed in both the quasi-static and dynamic collision post tests and the quasi-static and dynamic corner post tests were the essentially the same. However, in both tests there was an unexpected failure observed at the back of the collision post. The dynamic collision post test was nonetheless a success – the measured energy absorption of 138,000 ft-lbf exceeded the required value; the post deformed less than 10 inches into the occupied volume and did not separate from the end frame. However, in the subsequent quasi-static test, the premature fracture at the back of the post caused the load to drop enough that only 110,000 ft-lbf of energy was absorbed after 10 inches of permanent deformation. The significant difference in energy absorption made it difficult to definitively assert, based strictly on the results of the test, that the methods were equivalent.

Post-test analysis of the collision post tests revealed that the difference between the levels of energy absorption exhibited in the dynamic and quasi-static tests was likely due to the brittle nature of the fracture that occurred behind the post. Due to the high level of geometrical constraint against deformation in this region brought about by the internal gusset and the strap connection to the shelf, the fracture process was likely sensitive to local details in the design, such as the precise location of the welds and the extent of stress concentration in the weld regions (recall Figure 31).

The FE models, with and without material failure, clearly suggested that the two test methods resulted in similar modes of deformation and similar measures of energy absorption. Moreover, the excellent agreement between pre-test model predictions and test results for the corner post quasi-static load test suggested that, when the deformation and fracture modes were reasonably ductile, there was much less sensitivity to design details, and the behavior of the end structure was quite predictable. As long as this is the case, it is very likely that dynamic and quasi-static tests would yield similar results.

One can therefore conclude that the test methods were effectively equivalent; however, either test method could potentially be affected by details in the design and construction of the end frame that might cause it to exhibit brittle fracture modes or otherwise behave in such a manner that it exhibits sensitivity to such design details. In other words, the test methods were likely equivalent, but the behavior of a particular design may not be repeatable.

A third and final objective of this research was to implement the Bao-Wierzbicki material failure criterion in the FE models of the SOA end frame/M1 car retrofit and use the updated model to

predict the initiation and extent of material failure occurring in the three tests conducted in 2008 [6, 7]. The excellent agreement between model predictions and test results for the quasi-static corner post test clearly demonstrated that the material failure modeling effort proved successful. There are, however, a number of modeling and testing activities that could be undertaken to improve the effectiveness of the material failure model, including:

- A more comprehensive analysis of the effects of mesh refinement aimed at determining how best to keep the size of models manageable and how to keep mesh size sensitivity as low as possible.

- Additional analysis and testing aimed at providing a better understanding of how stress-strain behavior beyond the uniform elongation limit affect the initiation and growth of fractures and what material testing is needed to sufficiently characterize such behavior.

- A study of the extent to which material failure processes are different at structural connections than they are away from connections, and how such connections might be treated differently to improve the accuracy of models.

7. References

1. Bao, Y., and Wierzbicki, T. (2014). On fracture locus in the equivalent strain and stress triaxiality space. *International Journal of Mechanical Sciences*, *46*(1), 81–98.

2. Notice of Proposed Rulemaking. (August 2007). Passenger Equipment Safety Standards; Front-End Strength of Cab Cars and Multiple-Unit Locomotives. 49 CFR Part 238, Federal Register, Vol. 72, No. 147, 42016–42041.

3. APTA SS-C&S-034-99, Rev. 2. (2003). Standard for the Design and Construction of Passenger Railroad Rolling Stock. Vol. II – Construction and Structural, 11.0–11.44. American Public Transportation Association.

4. Mayville, R., Stringfellow, R., Martinez, E. (December 2006). Development of Conventional Passenger Cab Car End Structure Designs for Full-Scale Testing [DOT/FRA/ORD-06/20]. Washington, DC: U.S. Department of Transportation.

5. Martinez, E., Tyrell, D., and Zolock, J. (April 2003). Rail-Car Impact Tests with Steel Coil: Car Crush. *Proceedings of ASME/IEEE Joint Railroad Conference.* Paper No. JRC2003-1656.

6. Priante, M., Llana, P., Jacobsen, K., Tyrell, D., and Perlman, B. (September 2008). A Dynamic Test of a Collision Post of a State-of-the-Art End Frame Design. American Society of Mechanical Engineers, Paper No. RTDF2008-74020.

7. Muhlanger, M., Llana, P., and Tyrell, D. (March 2009). Dynamic and Quasi-Static Grade Crossing Collision Tests. *Proceedings of 2009 ASME Joint Rail Conference*. Paper No. JRC2009-63065.

8. HyperMesh. CAE Altair HyperWorks. Troy, MI.

9. ABAQUS Unified FEA – SIMULIA. Dassault Systemes, Johnston, RI.

10. Stringfellow, R. and Paetch, C (March 2009). Modeling Material Failure During Cab Car End Frame Impact. *Proceedings of 2009 ASME Joint Rail Conference.* Paper No. JRC2009-63054.

11. ASTM A370-19e1, Standard Test Methods and Definitions for Mechanical Testing of Steel Products (2019). ASTM International, West Conshohocken, PA.

12. ABAQUS User's Manual, Version 6.8. Volume III: Materials; Chapter 20: Progressive Damage and Failure.

13. Yu, H., Jeong, D.Y., Gordon, J.E., and Tang, Y.H. (September 2007). Analysis of Impact Energy to Fracture Un-Notched Charpy Specimens Made from Railroad Tank Car Steel. *Proceedings of the 2007 ASME Rail Transportation Division Fall Technical Conference.* RTDF2007-46038.

14. Tang, Y.H., Yu, H., Gordon, J.E., and Jeong, D.Y. (September 2008). Finite Element Analyses of Railroad Tank Car Head Impacts. *Proceedings of the 2008 ASME Rail Transportation Division Fall Technical Conference.* RDTF2008-74022.

15. Tang, Y, Yu, H, Gordon, J, Priante, M, Jeong, D, Tyree, D, and Perlman, A. (2007). Analysis of Full-Scale Tank Car Shell Impact Tests. *Proceedings of 2007 ASME Rail Transportation Division Fall Technical Conference.* RTDF2007-46010.

16. Tang, Y.H., Yu, H., Gordon, J.E., Priante, M., Jeong, D.Y., Tyrell, D.C., and Perlman, A.B. (September 2007). Analysis of Full-Scale Tank Car Shell Impact Tests. *Proceedings of the 2007 ASME Rail Transportation Division Fall Technical Conference.* RTDF2007-46010.

17. Tang, Y.H., Yu, H., Gordon, J.E., Jeong, D.Y., and Perlman, A.B. (April 2008). Analysis of Railroad Tank Car Shell Impacts Using Finite Element Method. *Proceedings of the 2008 IEEE/ASME Joint Rail Conference.* JRC2008-63014.

18. Lee, Y.-W. (February 2005). Fracture Prediction in Metal Sheets. Ph.D. Dissertation, Department of Ocean Engineering, Massachusetts Institute of Technology.

Abbreviations and Acronyms

ACRONYMS	EXPLANATION
APTA	American Public Transportation Association
CAD	Computer-Aided Design
TTC	Transportation Technology Center (the site)
TTCI	Transportation Technology Center, Inc. (the company)

Appendix A.   Design Specifications

1.0 INTRODUCTION

1.1. PURPOSE. The purpose of this specification is to define the requirements for the rail passenger cab car end structure to be fabricated onto an existing Budd M1 cab car.

1.2. DEFINITIONS.

1.2.1. Budd M1 Cab Car: The vehicle that the end structure will be installed on and will be use in the planned quasi-static and dynamic tests at TTCI in Pueblo, Colorado. The vehicles conform to the design defined by the drawings referenced in Section A.1.

1.2.2. Permanent deformation. There is technically no permanent deformation if a stress analysis shows that the Mises stress does not exceed the minimum specified yield strength.

2.0 REFERENCE DOCUMENTS/DRAWINGS

2.1. Budd M1 Drawings: (see attached list, Section A.1)

2.2. Standards:

2.2.1. AWS D1.1

2.2.2. APTA SS-C&S-034-99, Rev. 2, Standard for the Design and Construction of Passenger Railroad Rolling Stock, The American Public Transportation Association, Washington, D.C.

2.2.3. Code of Federal Regulations (CFR), Title 49, Part 238, various sections.

2.2.4. Notice of Proposed Rulemaking (NPRM), 49 CFR Part 238: "Passenger Equipment Safety Standards; Front-End Strength of Cab Cars and Multiple-Unit Locomotives," Subpart C— "Specific Requirements for Tier 1 Passenger Equipment," Federal Register Vol. 72, No. 147, August 1, 2007.

3.0 GENERAL DESCRIPTION

The cab car end structure, whose specifications are outlined in this document, is to be used in quasi-static and dynamic full-scale tests to be conducted in early to mid-2008. These tests will be used to investigate the collision performance of the end structure of a cab car in a simulated grade crossing collision. The end structure design will emulate the Budd Pioneer State-of-the-Art (SOA) end structure, whose corner post was previously tested and whose design is defined by the APTA SS-C&S-034-99 standard. The cab car equipped with this end structure will be tested either alone or in a consist representing a commuter train. The cab car will collide with a proxy object intended to simulate a heavy obstacle at a grade crossing. Following guidelines set out in the CFR Notice of Proposed Rulemaking, the proxy object will likely be a steel coil or a structure with similar weight and dimensions whose center of gravity is offset laterally from the centerline of the vehicle at the instant of collision with the collision post. In addition to the strength and energy absorption requirements, the car must also satisfy certain operational and physical requirements so that it could be used (mechanically) in actual service if incorporated into a modern rail coach car.

As noted in Section 2.2 above, many of the requirements in this specification are derived from the APTA SS-C&S-034-99 Standard and the CFR, Title 49, Part 238 related to Tier II equipment. Additional requirements related to the dynamic testing were derived from the CRF Notice of Proposed Rulemaking, Subpart C.

4.0 SPECIFIC REQUIREMENTS

4.1. STATE-OF-THE-ART END STRUCTURE REQUIREMENTS

4.1.1. Coupler

4.1.1.1. Coupler carrier. The coupler carrier shall be capable of resisting a downward force applied to the coupler shank of 100,000 lbf (445 kN) without permanent deformation of the supporting structure.

4.1.1.2. Buffer beam. The buffer beam above the coupler shall resist an upward force applied to the coupler shank of 100,000 lbf (445 kN) without permanent deformation of the buffer beam, supporting structure, and intervening connections.

4.1.2. End strength. The strength of the vehicle body shall be at least 800,000 lbf (3760 kN) without permanent deformation when the compressive load is applied to the centerline of draft. In addition, there shall be no permanent deformation of the car body structure when a 500,000 lbf (2240 kN) end-compression load is applied over an area not exceeding 6 inches (152 mm) high and 24 inches (610 mm) wide, centered vertically and horizontally on the underframe end sill or buffer beam construction.

4.1.3. Collision posts (see Figure A-1).

4.1.3.1. Description. There shall be two full height collision posts extending from the underframe to the cant rail or roofline. They shall be located at the approximate 1/3 points across the width of the vehicle and shall, in their entirety, be forward of the seating position of any crew member or passenger.

4.1.3.2. Strength. Each collision post shall resist each one of the following horizontal inward loads individually applied at any angle within 15 degrees of the longitudinal axis:

4.1.3.2.1. Minimum 500,000 pounds (2240 kN) applied at a point even with the top of the underframe, without exceeding the ultimate shear strength of the post (based on the shear area of the post which is depth of the post times the shear area of the webs).

4.1.3.2.2. Minimum 200,000 pounds (890 kN) applied at a point 30 inches (762 mm) above the top of the underframe, without exceeding the ultimate strength.

4.1.3.2.3. Minimum 60,000 pounds (267 kN) applied at any height along the post, including the top connection, above the top of the underframe, without permanent deformation of the post or supporting structure.

4.1.3.3. Energy Absorption. Each collision post shall be capable of absorbing energy under both quasi-static and dynamic loading conditions, as described below:

4.1.3.3.1. *Quasi-static loading*: Each collision post shall absorb a minimum of 135,000 ft-lbf (0.18 MJ) of energy when loaded longitudinally at a

height of 30 inches (762 mm) above the top of the underframe. The load may be applied over an area 6 inches (152 mm) high and wide enough to distribute the load directly into the post webs. At the moment that the collision post has absorbed this minimum energy:

- The post shall not permanently deflect more than 10 inches (254 mm) into the operator's cab or the passenger seating area.
- There shall be no complete separation of the post, its connection to the underframe, or its connection to the roof structure or the AT Plate (if used).

4.1.3.3.2. *Dynamic loading*: The front end structure shall be demonstrated to be capable of withstanding a frontal impact with a proxy object that is intended to approximate lading carried by a highway vehicle under the following conditions (see Figure A-2):

- The proxy object shall have a cylindrical shape, diameter of 48 inches (121.9 mm), length of 36 inches (91.4 mm), and minimum weight of 10,000 lbf (445 kN).
- The longitudinal axis of the proxy object shall be offset by 19 inches (483 mm) from the longitudinal axis of the cab car, which shall be ballasted to weigh a minimum of 100,000 lbf (445 kN).
- At impact, the longitudinal axis of the proxy object shall be 30 inches (762 mm) above the top of the finished floor; and
- The cab car and its end structure must withstand a 21 mph (9.9 m/s) impact with the proxy object resulting in no more than 10 inches (254 mm) of intrusion longitudinally into the occupied area of the vehicle without separation of the attachments of any structural members.

The areal dimensions of the collision posts, including any reinforcement required to provide the specified 500,000 pound (2240 kN) shear strength at the top of the underframe, shall extend from the bottom of the end sill to at least 30 inches (762 mm) above the top of the underframe. Each collision post and any shear reinforcement, if used, shall be welded to the top and bottom plates of the end sill with the equivalent of AWS pre-qualified welded joints.

4.1.4. Corner posts (see Figure A-1).

4.1.4.1. Description. The end structure shall have two structural corner posts, one located at each extreme corner of the car body structure. The corner posts shall extend from the bottom of the underframe structure to the bottom of the roof structure.

4.1.4.2. Strength. Each corner post, acting together with supporting car body structure, and intervening connections shall resist each of the following horizontal loads individually applied toward the inside of the vehicle in any direction from longitudinal to transverse:

4.1.4.2.1. Minimum 300,000 pounds (1334 kN) applied at a point even with the top of the underframe, without exceeding the ultimate shear strength of the post (based on the shear area of the post which is the depth of the post times the thickness of the webs).

4.1.4.2.2. Minimum 100,000 pounds (445 kN) applied at a point 18 inches (457 mm) above the top of the underframe, without permanent deformation.

4.1.4.2.3. Minimum 45,000 pounds (200 kN) applied anywhere between the top of the post at its connection to the roof structure, and the top of the underframe, without permanent deformation of the post or supporting structure.

4.1.4.3. Energy Absorption. Each corner post shall be capable of absorbing energy under both quasi-static and dynamic loading conditions, as described below:

4.1.4.3.1. *Quasi-static loading*: Each corner post shall be capable of absorbing a minimum of 120,000 ft-lbf (0.16 MJ) of energy when loaded longitudinally at a height of 30 inches (762 mm) above the top of the underframe. The load may be applied over an area 6 inches (152 mm) high and wide enough to distribute the load directly into the post webs. At the moment that the corner post has absorbed this minimum energy:
- The post shall not permanently deflect more than 10 inches (254 mm) into the operator's cab or the passenger seating area.
- There shall be no complete separation of the post, its connection to the underframe, or its connection to the roof structure or the AT plate (if used).

4.1.4.3.2. *Dynamic loading*: The front end structure shall be demonstrated to be capable of withstanding a frontal impact with a proxy object that is intended to approximate lading carried by a highway vehicle under the following conditions (see Figure A-2):
- The proxy object shall have a cylindrical shape, diameter of 48 inches (121.9 mm), length of 36 inches (91.4 mm), and minimum weight of 10,000 lbf (445 kN).
- The longitudinal axis of the proxy object shall be aligned with the outboard edge of the side of the cab car, which shall be ballasted to weigh a minimum of 100,000 lbf (445 kN).
- At impact, the longitudinal axis of the proxy object shall be 30 inches (762 mm) above the top of the finished floor; and
- The cab car and its end structure must withstand a 20 mph (9.4 m/s) impact with the proxy object resulting in no more than 10 inches (254 mm) of intrusion longitudinally into the occupied area of the vehicle without separation of the attachments of any structural members.

The areal dimensions of the corner post, including any reinforcement required to provide the specified 300,000 lbf (1334 kN) shear strength at the top of the underframe, shall extend from the bottom of the end sill to at least 30 inches (762 mm) above the top of the underframe. Each corner post and any shear reinforcement, if used, shall be welded to the top and bottom plates of the end sill with the equivalent of AWS pre-qualified welded joints.

4.1.5. Horizontal Framing Members (see Figure A-1).

4.1.5.1. Description. There shall be a horizontal structural member between the collision post and the corner post on each side at a height equivalent to the bottom of the windshield.

4.1.5.2. Strength. The structural member shall support a minimum load of 15,000 lbf applied transverse to the member at any point on its span without permanent deformation of any part of the vehicle structure.
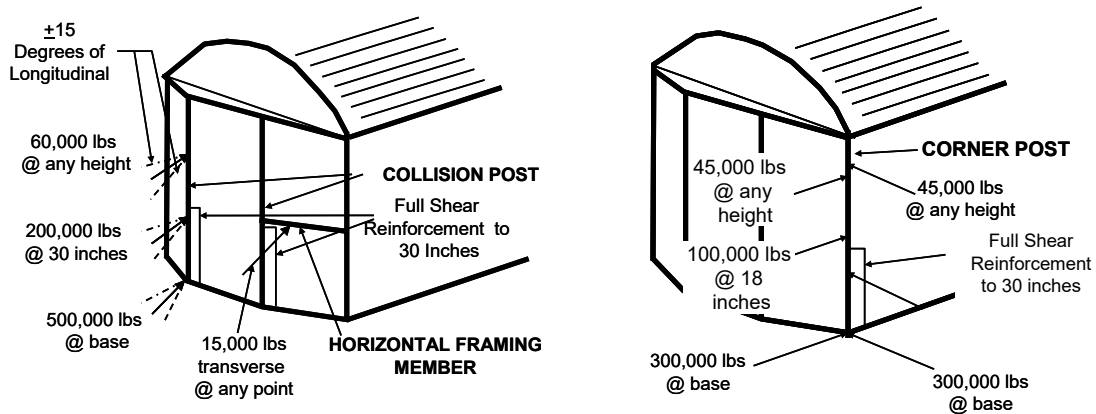
Figure A-1. Schematic of the collision post, corner post and horizontal framing member requirements

Figure A-2. Schematic of dynamic collision post performance collision scenario

4.2. OPERATIONAL REQUIREMENTS

4.2.1. Coupler system.

4.2.1.1. Coupler. The coupler shall be a Type H tightlock coupler. There is no specific requirement on shank length except that it must be compatible with the other requirements of this specification.

4.2.1.2. Coupler carrier.

4.2.1.2.1. Adjustment requirements. There shall be a spring-loaded coupler carrier to maintain the coupler in the horizontal position when uncoupled.

4.2.1.3. Draft gear.

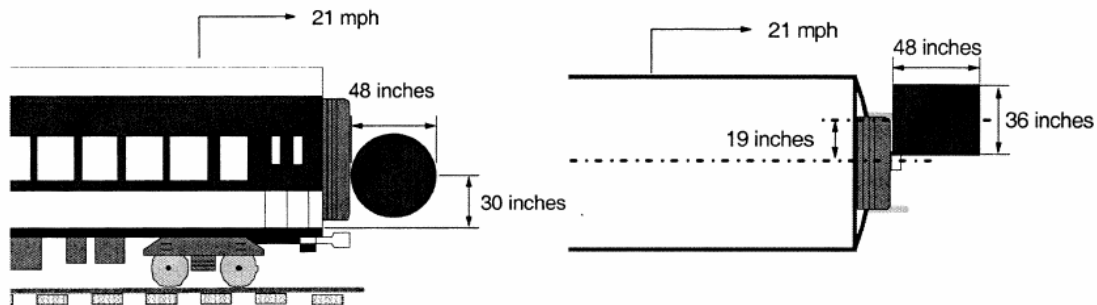4.2.1.3.1. General. The coupling system shall include a draft gear capable of absorbing low speed impacts.

4.2.2. Uncoupling. The vehicle end shall be equipped with an AAR Style No.6 uncoupling mechanism.

4.3. TEST REQUIREMENTS

4.3.1. General. The vehicle end designed and built to this specification will be used for full-scale testing. Therefore, it is important that the design facilitate measurements and observations to be made during the tests. The types of tests envisioned include: a single vehicle colliding with a heavy object mounted on a rigid surface to simulate a grade crossing collision, or a vehicle end-loaded with a heavy object colliding with a single vehicle with this end structure. The tests will be conducted at TTCI in Pueblo, Colorado.

4.3.2. Visibility. The vehicle end shall be designed in such a way that it will be possible to view the collision and corner posts during deformation in the test. For example, parts of the roof and sides must remain open to facilitate viewing by cameras mounted on the ground or on the vehicle.

4.4. FABRICATION REQUIREMENTS

4.4.1. General. The design should utilize materials and fabrication methods that a normal metal fabrication company could use.

4.4.2. Materials and construction methods

4.4.2.1. Materials. The materials of construction for the primary structure and the energy absorbing elements shall be either high strength low alloy (also known as low-alloy, high tensile) or austenitic stainless steels commonly used in the fabrication of modern railway vehicles for operation in North America.

4.4.2.2. Construction Methods. All primary structural members shall be welded in accordance with AWS D1.1.

4.4.3. Overall vehicle integration. The end structure shall be designed so that it can be integrated into the existing Budd M1 cab car. The goal of the design shall be to minimize the amount of effort required for installing the end structure onto the existing car.

4.5. PHYSICAL REQUIREMENTS:

4.5.1. Envelope. The end structures are to be attached to the end of one of the existing Budd M1 cab cars. Its outer boundaries should not exceed those of the as-built Budd M1 cars with the possible exception of the length beyond the bolster center point.

4.5.2. Curving. The components of the vehicle end shall not interfere for operation with nominally identical cars operating on curves as tight as a 250 foot radius.

4.5.3. Space for normal equipment. Although much of the usual equipment found on passenger rail cars will not be included in this design, the design shall provide

space for this equipment. Openings, piping and other components normally associated with this equipment need not be included. The equipment not already specified includes:

- Hand brake
- HEP (head end power)
- 27-point communication line
- Trainline box
- Electronic brake box
- Diaphragm

A.1. Budd M1 Car Drawings

1. B01-23818   End Underframe B-End
2. B01-23955   End Underframe F-End
3. B12-04548C   Center Sill Assembly
4. B42-05927   Weld Arrangement – Side Frame to Floor
5. B42-05928 Lot 37A Weld Arrangement – Side Frame to Floor at Crossbearer
6. B42-05928 Lot 37B Weld Arrangement – Side Frame to Floor at Crossbearer
7. B42-05929 Lot 37A Door Weld Arrangement
8. B42-05929 Lot 37B Door Weld Arrangement
9. B42-05958   Weld Arrangement (Top Level)
10. B47-15252   Floor to Side Sill Details – Detail Circle 8-12
11. B47-15252   Floor to Side Sill Details – Detail Circle 13-15
12. B47-15252   Floor to Side Sill Details – Detail Circle 17
13. B47-15252   Floor to Side Sill Details – Detail Circle 22-23
14. B48-10956   Typical Weld at Roof – Detail 2
15. B48-10956   Typical Weld at Roof – Detail 3
16. B48-10956   Typical Weld at Roof – Detail 6
17. B48-10956   Typical Weld at Roof – Detail 8
18. B48-10956   Typical Weld at Roof – Detail 10
19. B48-10956   Typical Weld at Roof – Detail 13
20. D01-23886   Bolster Channel – Side
21. D01-23887   Bolster Channel – Side
22. D02-26819-830   Post Channel
23. D47-15252   Typical Sections and Details Floor – Center Sill to Underframe Connection – Detail Circle 1
24. D47-15252   Typical Sections and Details Floor – Center Sill to Underframe Connection – Detail Circle 2
25. D47-15252   Typical Sections and Details Floor – Center Sill to Underframe Connection – Detail Circle 16
26. D47-15252   Typical Sections and Details Floor – Center Sill to Underframe Connection – Detail Circle 18-19
27. D47-15252   Typical Sections and Details Floor – Center Sill to Underframe Connection – Detail Circle 20-21
28. D47-15252   Typical Sections and Details Floor – Center Sill to Underframe Connection – Detail Circle 25
29. D47-15252   Typical Sections and Details Floor – Center Sill to Underframe Connection – Detail Circle 26-27
30. D47-15252   Typical Sections and Details Floor – Center Sill to Underframe Connection – Detail Circle 28-29
31. D47-15252   Typical Sections and Details Floor – Center Sill to Underframe Connection – Detail Circle 30
32. D47-15252   Typical Sections and Details Floor – Center Sill to Underframe Connection – Detail Circle 31
33. D47-15252   Typical Sections and Details Floor – Center Sill to Underframe Connection – Detail Circle 32

Appendix B. Detailed Design Drawing List

Drawing Number	Drawing Title or Part Name	Revision	Date
D038-009-001	M1 CAR PREPARATION	A	7-Apr-09
D038-009-002	M1 CAR REINFORCEMENT	A	7-Apr-09
D038-009-003	END FRAME INSTALLATION	A	7-Apr-09
D038-009-010	END FRAME ASSEMBLY	D	7-Apr-09
D038-009-011	SIDE SILL CHANNEL TOP - RH	A	7-Apr-09
D038-009-012	SIDE SILL ANGLE BOT - RH	A	7-Apr-09
D038-009-013	SIDE SILL ANGLE BOT - LH	A	7-Apr-09
D038-009-014	DRAFT SILL ANGLE		6-Dec-07
D038-009-015	SIDE SILL EXTENSION CHANNEL	A	10-Mar-08
D038-009-016	SIDE SILL EXTENSION GUSSET	A	10-Mar-08
D038-009-017	TRANSFER PLATE		6-Dec-07
D038-009-018	ROOF RAIL BRACE	A	7-Apr-09
D038-009-019	ROOF RAIL TUBE ASSY.		6-Dec-07
D038-009-020	ANGLE		6-Dec-07
D038-009-021	ANGLE		6-Dec-07
D038-009-022	ROOF RAIL GUSSET		6-Dec-07
D038-009-023	TUBE CONNECTOR		6-Dec-07
D038-009-024	POST CONNECTION PLATE		6-Dec-07
D038-009-025	ROOF RAIL EXTENSION PLATE		6-Dec-07
D038-009-026	ROOF RAIL EXTENSION ANGLE - RH		6-Dec-07
D038-009-027	BRACE CONNECTION GUSSET		6-Dec-07
D038-009-028	FACE PLATE PAD		6-Dec-07
D038-009-029	DRAFT SILL WEDGE		6-Dec-07
D038-009-030	DIAGONAL BRACE		6-Dec-07
D038-009-031	SIDE SILL ANGLE MID		6-Dec-07
D038-009-032	BACKING ANGLE	A	6-Dec-07
D038-009-033	ROOF RAIL EXTENSION ANGLE - LH		18-Jan-08
D038-009-034	TRANSFER PLATE		6-Dec-07
D038-009-035	HORIZONTAL CONNECTION TUBE		6-Dec-07
D038-009-036	SIDE SILL CHANNEL TOP - LH	A	7-Apr-09
D038-009-037	CHANNEL POST CLIP ANGLE - LH		6-Dec-07
D038-009-038	CHANNEL POST CLIP ANGLE - RH		18-Jan-08
D038-009-039	HAT POST FLANGE EXTENSION		6-Dec-07
D038-009-040	UNDERFRAME GUSSET		6-Dec-07

Appendix C. Quality Control Requirements

Introduction

This document covers the minimum quality control requirements for components and assemblies for three end frames and supporting structures, with:

- Materials supplied by and components fabricated by Zimmerman Metals, Inc. in Denver, CO.
- Welding and assembly at TTC, according to TRA drawings D038-009-010 through D038-009-040.

One of the primary objectives of this quality control process for this program is to ensure that the proper quantity of parts is received at TTC and that each part is:

- Properly labeled
- Dimensioned according to specifications spelled out in the drawings
- Traceable to a specific material certification report

A second objective the quality control process for this program is to ensure that the end frames are assembled and welded according to the specifications spelled out in drawings as well as standard welding practice.

Parts fabricated at Zimmerman are to be inspected by a member of the TIAX team and/or personnel from TTC. To the extent possible, this inspection should take place at Zimmerman prior to shipment of the parts.

Particular areas deserving quality control by the team are:

- Ensure bevels are correctly included on piece parts.
- Make sure long items satisfy the straightness requirements of the drawing.

General

Material Certifications

- There must be a material certification associated with each part used in the fabrication of the end frames and supporting structures.
- Material certifications for backing bars are not required.

Part Identification

- Each part must be marked for identification with the part number. A scheme for marking the parts has been devised and is shown at the end of this appendix.

Welding

- Welding is to be conducted according to the AWS D15.1 standard.

<u>Measurement Instrumentation</u>

- All instruments used to make measurements reported in the quality control documentation must be calibrated within the last year.

- Written records of incoming inspection and dimensional measurements and checks will be provided as part of the QC report.

<u>Photographic Documentation</u>

Each assembly or weldment is to be photographed in such a manner that there are views of the internal components, when applicable, and of the finished assembly from several perspectives. That is, photographs should be taken on each side, and on top and bottom when the detail of the assembly requires it. Photographs should be clear, in focus and identified (by vehicle end). A marking on the part being photographed is sufficient for identification. The photographs should be provided in digital form on a CD in folders representing each vehicle end. Note: the primary purpose of this requirement is to document details that will not be visible once the entire assembly is fabricated.

Requirements Particular to Drawings
Note: All dimensions on the drawings should be checked, including specified tolerances. The purpose of the list that follows is to identify the most critical dimensions.

<u>Drawing -010, End Frame Assembly</u>

- Distance from assembly centerline to collision and corner post centerlines, main view measure at top and bottom
- Distance from top of end beam to underside of AT beam at three locations: sides and center (6 – 3 9/16")
- Straightness of finished end beam (in two planes
- Straightness of finished AT beam (in two planes)
- Holes in buffer beam, AT channel, and their top plates to be positioned as shown in the drawing. Dimensions given are after bending, when applicable.

Inspection of Fabricated Parts

The spreadsheets that accompany this document ("Volpe M1 SOA QC Inspection.xls") should be used to conduct the inspection of fabricated parts. The individual conducting the inspection should place his/her initials in the appropriate locations.   Note that backing bars do not require material certifications. In addition, it is not required that all backing bars be inspected for dimensional accuracy – it is sufficient to inspect one representative backing bar for each item in the list of parts. Accordingly, there is only one row provided for inspection of such parts; however, the inspector must ensure that all of the parts are properly marked and delivered to TTC.

MARKING OF FABRICATED PARTS

The objective of this numbering scheme is to ensure each part delivered has a marking that clearly corresponds to its drawing.

For parts from drawing D038-009-010 ("END FRAME ASSEMBLY") – use drawing number followed by "item".

e.g.,   for item 5 on drawing D038-009-010 ("BUFFER BEAM GUSSET"):

→ Marking to read: **010 item 5**

(Since the QTY is "4" for this part and 3x sets of parts are required, there will be a total of twelve (12) parts with this same marking.)

For parts from 11 x 17 drawings (011 to 040) – use rightmost 3 digits of drawing number:

e.g.,   for part number D038-009-014 (DRAFT SILL ANGLE):

→ Marking to read: **014**

(Since the QTY is "2" for this part, there will be a total of two (2) parts with this same marking.)

For plates that are not drawn, but called out in drawings D038-009-002 and 003, use drawing number followed by "item".

e.g.,   for item 21 on drawing D038-009-002 ("SIDE SILL WEB PLATE"):

→ Marking to read: **002 item 21**

(Since the QTY is "3" for this part, there will be a total of three (3) parts with this same marking).

Appendix D. Material Failure Model

D.1   MODEL DEVELOPMENT

It is recognized that material failure is dependent not only on the extent that a material is strained beyond its yield point but also on the nature of the stress that accompanies that strain. For example, materials generally can sustain much higher levels of stress in compression than they can in tension. Intuitively, a stress state that tends to pull a material apart tends to promote fracture of that material. This phenomenon is most often characterized through the triaxiality, Σ, of the stress state:

$$\Sigma = \sigma_m / \sigma_e,$$

where σ_m is the mean stress (the average of the three principal stresses) and σ_e is the von Mises stress (a measure of the magnitude of the stress).

Using the Bao-Wierzbicki criterion, failure initiates when the deformation of the structure induces plastic strain levels that exceed threshold values that are dependent on Σ, as illustrated in Figure D-1. The solid line defines a plastic strain- and triaxiality-based failure envelope in which damage initiates when the plastic strain exceeds the value defined by the curve. The unique shape of the line shown in Figure D-2 is a fundamental characteristic of the Bao-Wierzbicki criterion. It is derived from a fit to the results of many tests that were conducted at different triaxiality levels and accounts for the different modes of fracture that may occur, as indicated. It is characterized by two parameters, C_1 and C_2, the fracture initiation strains for conditions of pure shear and uniaxial tension, respectively. (Note that the C_1 and C_2 parameters are not independent – they are proportional and related to one another by a material hardening exponent, as is described in [3].)
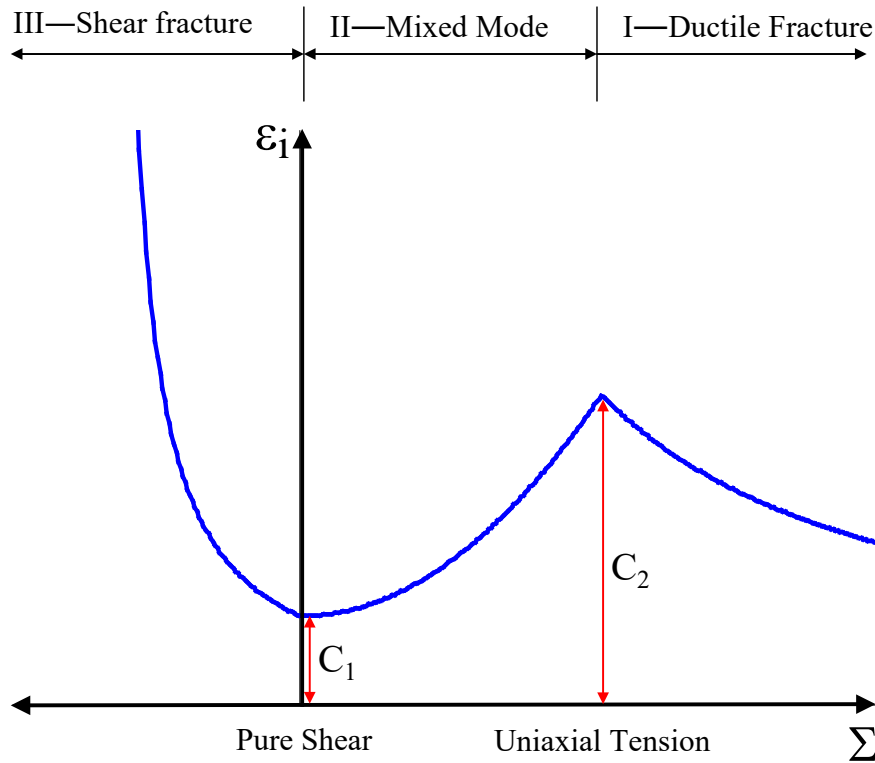
Figure D-1. Schematic illustration of the Bao-Wierzbicki triaxiality-dependent failure initiation criterion

The material model for the end frame structural elements was implemented in ABAQUS/Explicit using the Johnson-Cook plasticity model. The Bao-Wierzbicki failure criterion was defined using the "*DAMAGE INITIATION" material parameter option.

As is shown schematically in Figure D-2, once failure initiates, the local strength of the material is assumed to decrease from its value at the fracture initiation strain, ε_i. The plastic strain at which the material strength decreases to zero is referred to as the failure strain, ε_f, as indicated in Figure D-2. In ABAQUS, this behavior is defined through the "*DAMAGE EVOLUTION" material parameter. For reasons that are related to minimization of mesh-dependencies, and are described in detail in [12], the plastic strain at failure is described indirectly through definition of a plastic deformation at failure parameter, u_f. The strain rate $\dot{\varepsilon}_{pl}$ following fracture initiation is defined to be proportional to the displacement rate $\dot{u}_{pl}$ such that:

$$\dot{u}_{pl} = L_e \bullet \dot{\varepsilon}_{pl},$$

where L_e is a characteristic length for elements near the location of fracture.
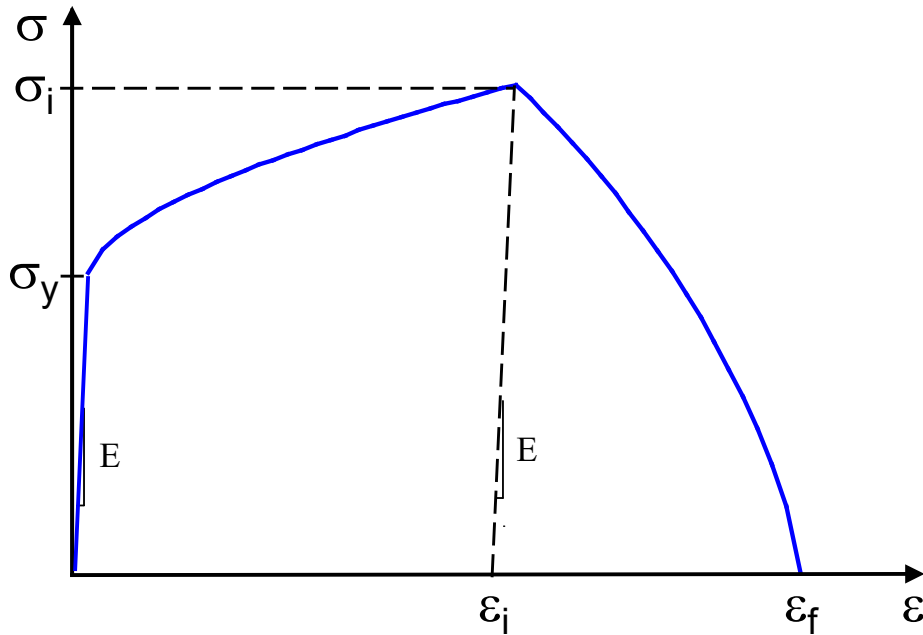
Figure D-2. Stress-strain curve with damage evolution following initiation of material failure

A test problem meant to be representative of the mechanics that govern the impact of a coil-shaped object into a corner post or a collision post was chosen to evaluate several aspects of the material failure model and determine how best to apply the model to the simulations of the full-scale tests. A schematic of the test problem is shown in Figure D-3. In this problem, the transverse impact of a 48-inch-diameter rigid coil moving at 21 mph into the center of a 76-inch-high post, fully-supported at both ends, is simulated. (Symmetry allows for modeling of only $1/4^{th}$ of the beam.) Despite the simplified nature of the test problem, the all-solid mesh illustrated in Figure D-3, which has only 4 elements through the thickness of the post members, uses over 220,000 elements. It would not be practical to create an entire endframe model using solid elements. Note that, following [13], elements with equal lengths in all dimensions (e.g., cubic-shaped for solid elements and square-shaped for shell elements) were used when modeling material failure in order to reduce mesh dependencies.)

Due to the practical numerical limitations of solid element-only models, the use of shell-to-solid coupling was next investigated. This method, used by Tang et al. [14] in the tank car impact study, allows for the use of solid elements in the area around the failure location and shell elements away from the failure location. With the interface of the solid-meshed and shell-meshed regions of the structure properly defined, appropriate kinematic constraints are automatically applied. Studies were conducted to evaluate the effect of: (1) the size of the solid-element region; and (2) the refinement of the mesh.
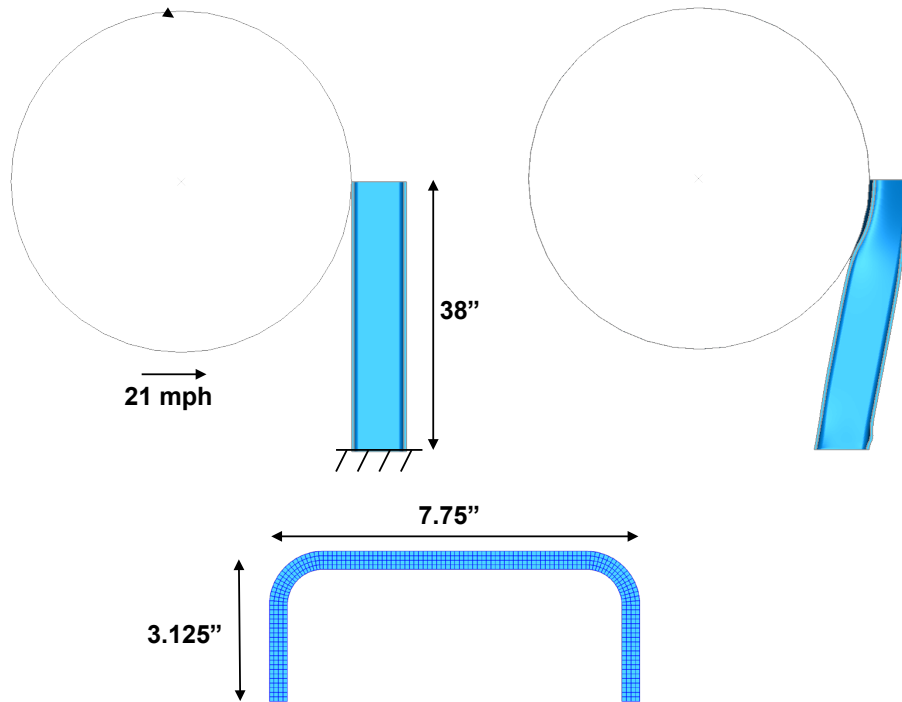
Figure D-3. Schematic illustration of the coil impact test problem

The results of these studies indicate that the size of the solid region needs to be large enough so that fracture processes do not interact with the solid-to-shell interface. Otherwise, the results are not strongly affected. For example, if the solid region is 6.25 inches high, the predicted energy absorbed by the post prior to fracture is only about 2.5 percent higher than it is when the solid region is 3.125 inches high. Meanwhile, the number of elements in the mesh drops significantly. On the other hand, an evaluation of the effect of mesh density indicates that increasing the number of elements through the thickness of the post members from 4 to 8, as shown in Figure D-5, decreases the energy absorbed at fracture by over 20 percent.
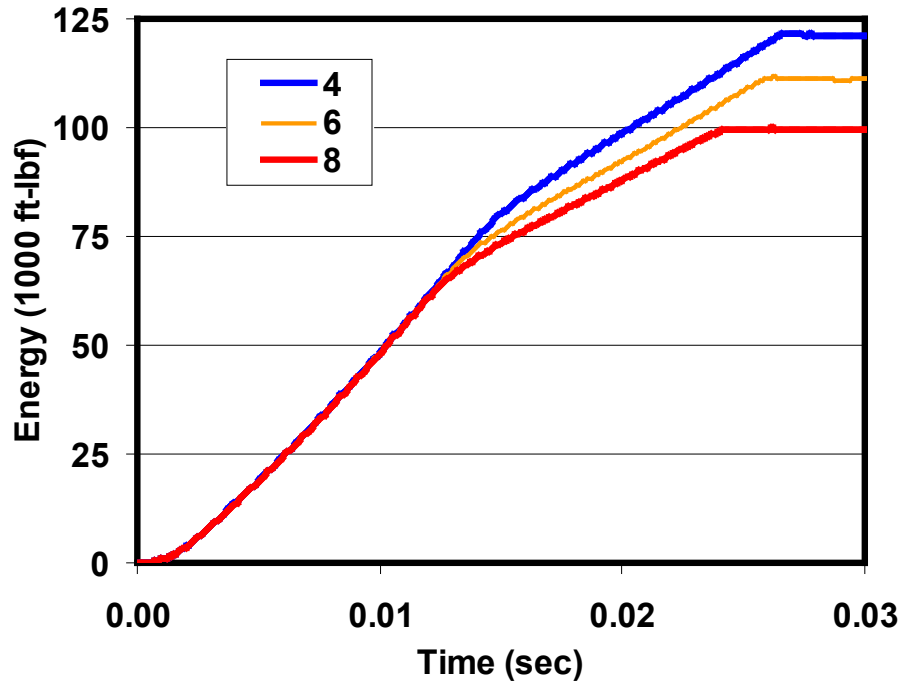
Figure D-4. The effect of mesh refinement on the time-history of energy absorption for the test impact problem. The number of elements through the thickness of the post members is indicated.

Preliminary analyses indicated that refined meshes were required in the regions of failure. This requirement, coupled with the potential for multiple failure sites, makes shell-only meshes more attractive than mixed solid/shell meshes for modeling the impact and large deformation of cab car end structures. (Shell-element models are computationally much less expensive than solid-element models). In addition, some of the interfaces between structural elements are quite complex, and the connections between the collision/corner posts and the end beam are gusseted. The presence of the gussets makes it very difficult to properly define the kinematic constraints at the shell/solid interface.

In ABAQUS, the failure modeling capability for ductile metals can be used with any element type that includes mechanical behavior. Problems like the punch-through of the tank car head studied in [14–17] must be analyzed with solid elements, because the stress state during failure is dominated by through-thickness shear. However, when the structures are shell-like, and the stress in those structures is characterized by in-plane tension or compression, there is no inherent reason that shell elements cannot be used to model failure. One must take care that, when applying material parameters to use with shell elements, they been validated specifically for use with shell elements because the stress and strain patterns that arise near the locations of failure are different for these two element types.

Validation of the Bao-Wierzbicki failure criterion, and in fact any triaxiality-based criterion, for use with shell elements is complicated by the fact that, for these elements, the through-thickness

stress is by definition equal to zero. For this reason, the stress triaxiality is limited to the range –2/3 to +2/3. As long as the state of stress is truly biaxial, this does not appear to present any difficulties. However, in conditions where there is a sizable through-thickness stress, the definition of the triaxiality dependence of the failure initiation strain becomes problematic. This situation arises when, for example, the region of failure is near a relatively rigid connection, such as that between the bottom of a collision or corner post and the end beam. For example, even with a great deal of mesh refinement, a shell element model may not pick-up what is likely to be an increase in the through-thickness stress just near a rigid connection, where failure may initiate. (It is worth noting that solid element models have similar issues at rigid connections.)

To evaluate the use of a shell element-only model with material failure, the solid or mixed solid/shell mesh for the coil impact test problem was replaced with a shell-only mesh with the same characteristic element size – 0.09 inch. Initial calculations using identical failure parameters indicated that the shell-only model predicts a level of energy absorption that is about 45 percent less than the corresponding mixed solid/shell model. Inspection of the region where failure first initiates, as shown in Figure D-5, reveals that the plastic strain distribution in the solid/shell and shell-only models is similar, but the peak strain levels are higher (30 percent vs. 15percent) for the shell-only models, due to the manner in which the loads are accommodated at the connection.
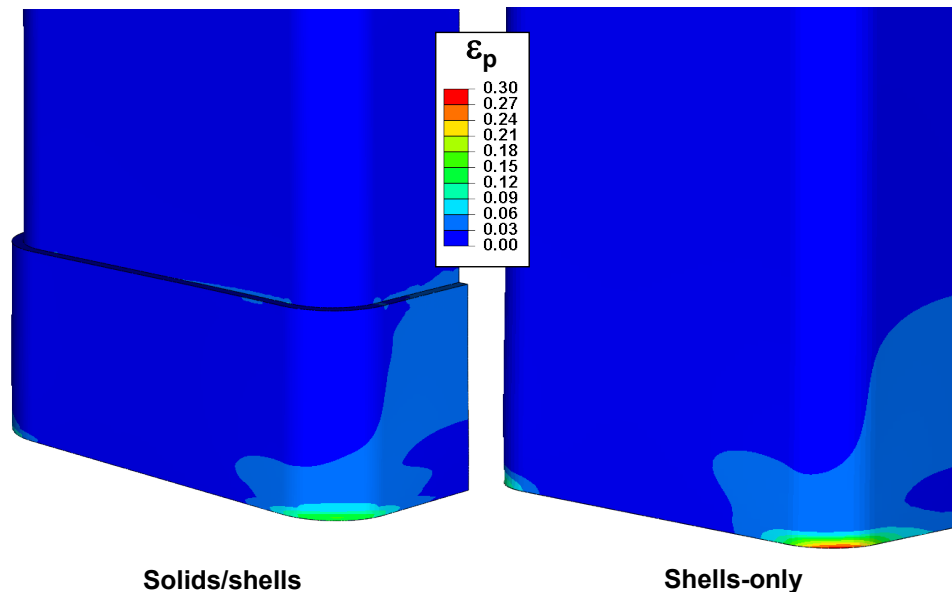

Figure D-5. Comparison of strain distributions in solid/shell and shell-only models at base of post just prior to fracture initiation

In addition to the different peak plastic strain levels, the triaxiality of the stress state in this region is different for the two types of models, as illustrated in Figure D-6. In both types of models, the triaxiality builds up and maintains an effectively constant level through the failure process. However, the level of triaxiality is significantly higher for the shell-only model.
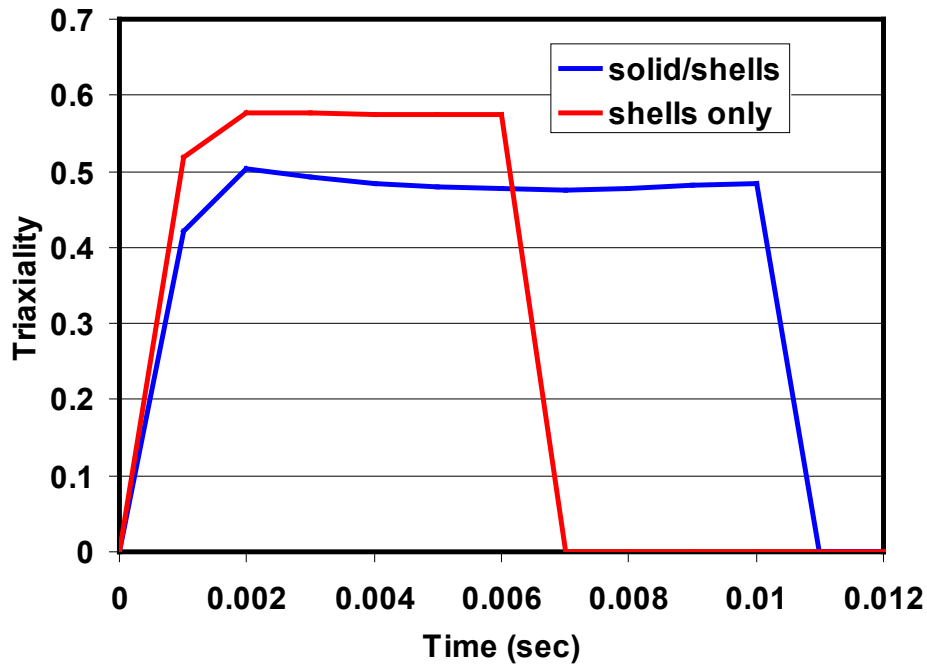
Figure D-6. Comparison of triaxiality histories at the location of failure initiation for the solid/shell and shell-only models

Because of the higher strain and triaxiality levels, complete failure of the post occurs much earlier in the shell-only models, thus the much smaller energy absorption. However, if the key Bao-Wierzbicki parameters C_1 and C_2 are modified (recall that they are proportional to one another), effectively raising or lowering the threshold failure curve shown in Figure D-1, the behavior of the solid/shell and shell-only models can be made to be nearly identical. Figure D-7 compares the deformation of the post for both a solid/shell model and a shell-only model just prior to complete failure and reveals that the deformed shapes are essentially identical. The failure models for these two cases differ only by the magnitude of the C_1 and C_2 parameters. For this comparison, the C_2 parameter was set at 0.45 for the shell-only model, and 0.19 for the solid/shell model (the C_1 parameters were scaled accordingly). The energy absorption time-histories are also consistent, as shown in Figure D-8. It is worth noting that the value of the C_2 parameter used in both models is significantly lower than the value of 1.08 that was experimentally determined for A710 steel [18]. This difference likely reflects an influence of stress concentration at the connection on the failure process
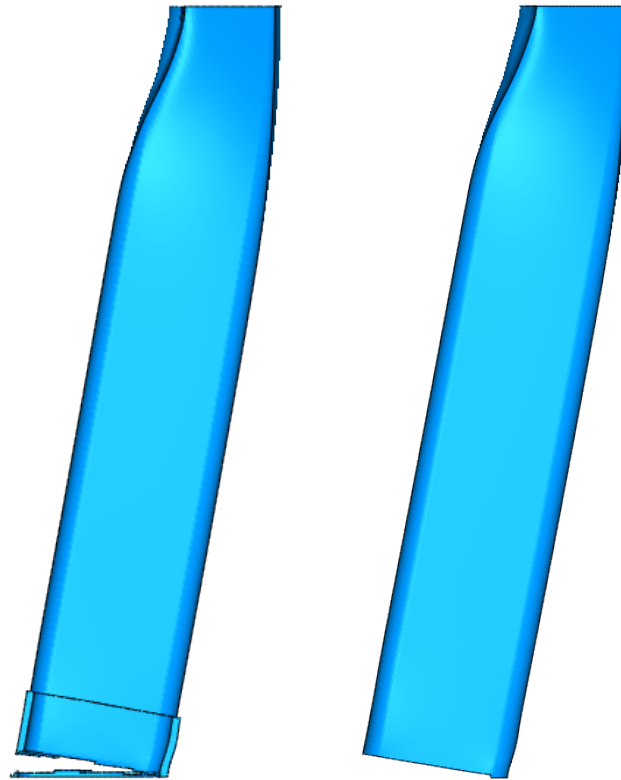
Solids/shells   **Shells-only**

Figure D-7. Comparison of post deformation just prior to complete failure for the solid/shell and shell-only models
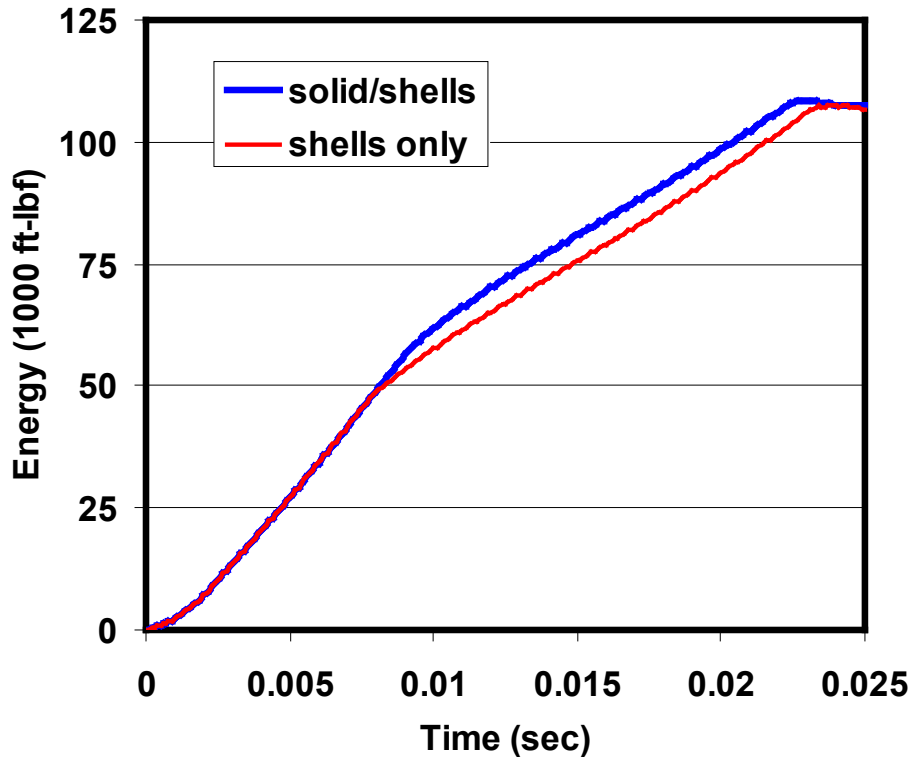
Figure D-8. Comparison of post energy-absorption time-histories for the solid/shell and shell-only models

D.2   MODEL VALIDATION

A shell-only model of the cab car end frame was constructed and is pictured in Figure D-9. The model contains approximately 160,000 elements, with an element size of approximately 1.0" away from the regions where failure may occur. The mesh is refined to an element size of refined 0.125 inch in the failure regions. The remainder of the vehicle was assumed to behave as a rigid mass. Preliminary calculations demonstrated that this assumption resulted in only minor changes to model predictions. Material failure parameters were adjusted by comparison to the results of the dynamic coil impact test of the corner post of the SOA end frame, which was conducted at TTC in June 2002 [5]. The corner post of the SOA end frame deflected about 10 inches due to impact of a 40,000-lbm, 6-ft-diameter by 4-ft-wide steel coil traveling at 14 mph, with the post fracturing in a few locations, but remaining attached to the end frame. A photograph of the base of the post following the test is shown in Figure D-10.
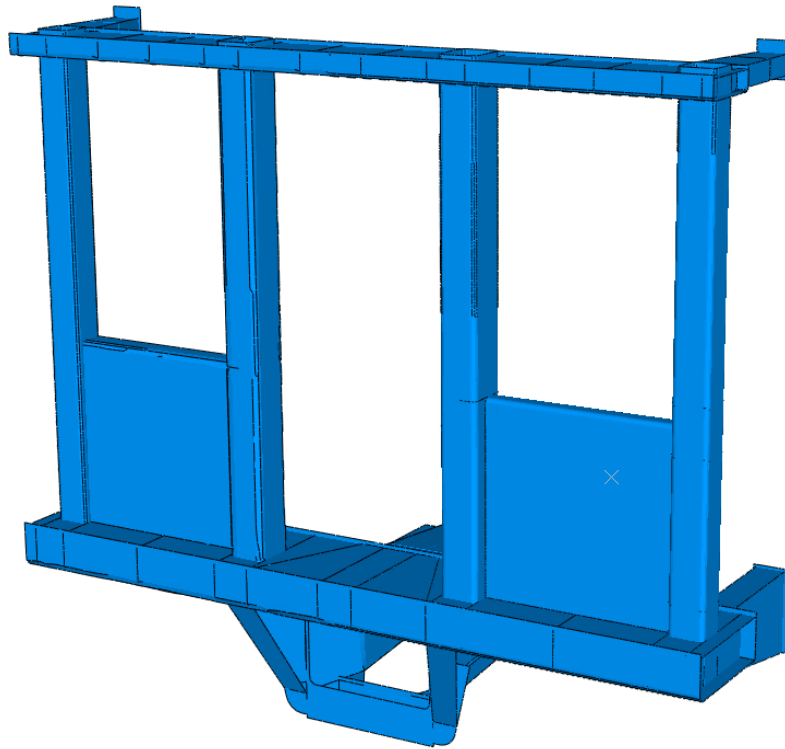
Figure D-9. The finite element mesh for the cab car endframe

Figure D-10. Post-test photograph of base of corner post following coil impact

Using measured strength parameters for A710, the steel from which the end frame was constructed, material failure parameters (namely, failure initiation parameters C_1 and C_2, and the plastic deformation at failure parameter, u_f) were modified to best capture the extent of fracture at the base of the post. The deformed end frame mesh following the simulated impact is shown in Figure D-11 and is consistent with the actual extent of fracture and deformation shown in Figure D-10.
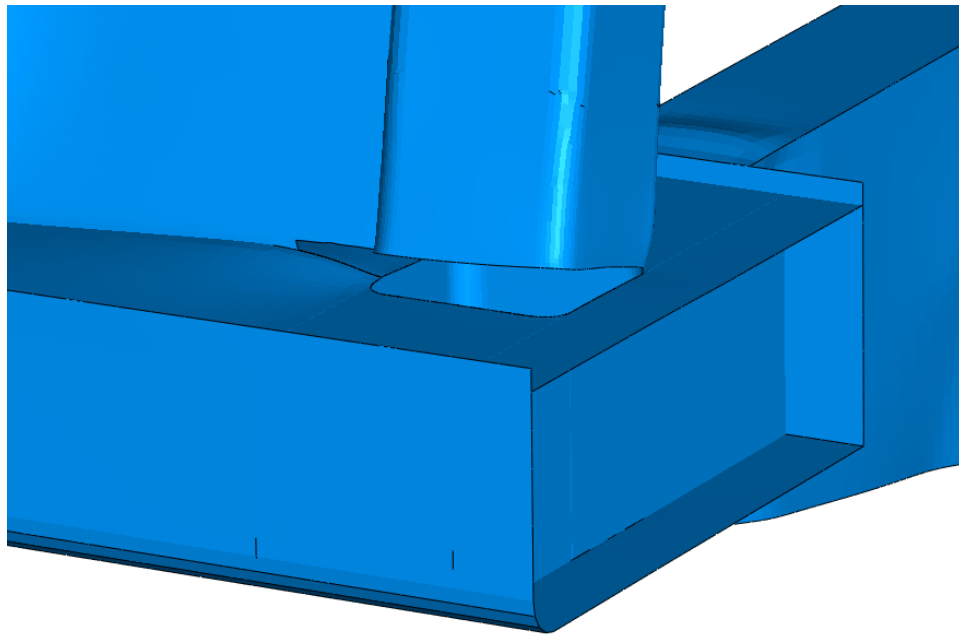

Figure D-11. Predicted deformation of end frame following coil impact

The predicted force-time history is compared with measured data in Figure D-12 and appears to be consistent with test results. The predicted penetration of the coil is about 10.8 inches, as compared with 10.2 inches that were measured.
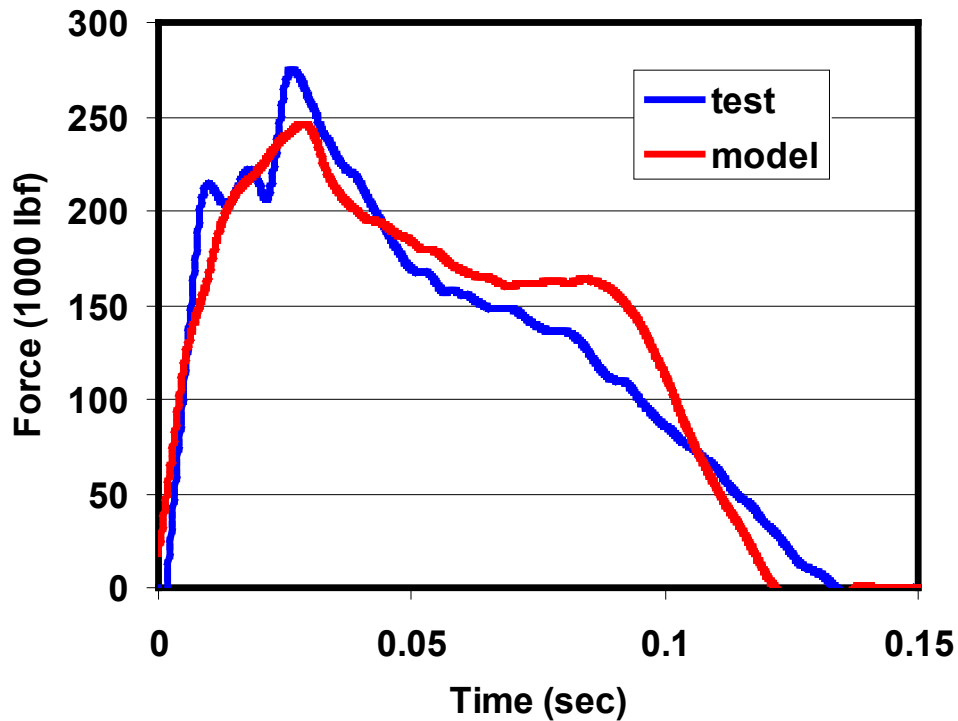
Figure D-12. Comparison of predicted and measured coil force-time histories

D.3 CONCLUSIONS

A material failure model, based on the Bao-Wierzbicki criterion, was successfully implemented into ABAQUS for use with shell elements. Model development efforts indicate that the shell elements can be effectively used to model material failure. Moreover, it appears that the nature of the cab car end frame crush problem is such that the use of shell elements only is likely more effective than a mix of solids and shells.

The application of the model in simulations of the full-scale tests of cab car end frames demonstrates that material failure modeling can be an effective tool that increases the accuracy of pre-test predictions. For cases where fracture is likely, such models are very likely more accurate predictions of behavior than models that do not account for failure. It is evident, however, that there are potential pitfalls that must be avoided when evaluating model predictions. One lesson that was learned in this study is that these models lose much of their effectiveness when the fracture process is strongly influenced by complex structural details, such as the gusseted, strapped, and welded connection of the original design of the shelf connection to the collision post. In such cases, it may be difficult with shell elements only to capture important structural details that may have a significant effect on the fracture behavior of the structure, and shell element-only models lose some of their effectiveness.

When such complexities are avoided, it appears as though, with some effort given to characterizing the failure properties of the materials and validating the material parameters, very

effective models which account for material failure can be constructed and used to aid the design process and evaluate structural behavior.

One aspect of the problem that warrants additional study is the selection of the key failure parameters C_1 and C_2. It appears that when the failure parameters are optimized to predict failure at a connection (in our case, the front base of the post), they may not be optimal for failure in regions where there is no connection. In the model, the details of the connection are idealized, and the concentrated stress state that arises at the connection may not match the conditions in the actual structure. Away from connections, this issue isn't present, and it is more likely that the material parameters match measured values. For this same reason, there is likely to be more mesh-size dependence for a failure near a connection. Methods to account for such differences in conditions would allow the models to be less dependent on validation and therefore more widely applicable.